END

FILMED

DTIC

REPORT DOCUMENTATION PAGE		READ INSTRUCTIONS BEFORE COMPLETING FORM
1. REPORT NUMBER SM 85-14	2. GOVT ACCESSION NO.	3. RECIPIENT'S CATALOG NUMBER
4. TITLE *(and Subtitle)* "DYNAMIC FRACTURE IN VISCOELASTIC SOLIDS"		5. TYPE OF REPORT & PERIOD COVERED Final Report
		6. PERFORMING ORG. REPORT NUMBER
7. AUTHOR*(s)* W.G. Knauss		8. CONTRACT OR GRANT NUMBER*(s)* ONR N00014-78-C-0634
9. PERFORMING ORGANIZATION NAME AND ADDRESS California Institute of Technology Pasadena, CA 91125		10. PROGRAM ELEMENT, PROJECT, TASK AREA & WORK UNIT NUMBERS
11. CONTROLLING OFFICE NAME AND ADDRESS Office of Naval Research		12. REPORT DATE June 30, 1985
Mechanics Division, Code 473 Arlington, VA 22217		13. NUMBER OF PAGES 55
14. MONITORING AGENCY NAME & ADDRESS*(if different from Controlling Office)*		15. SECURITY CLASS. *(of this report)* UNCLASSIFIED
		15a. DECLASSIFICATION DOWNGRADING SCHEDULE
16. DISTRIBUTION STATEMENT *(of this Report)*		
17. DISTRIBUTION STATEMENT *(of the abstract entered in Block 20, if different from Report)*		
18. SUPPLEMENTARY NOTES		
19. KEY WORDS *(Continue on reverse side if necessary and identify by block number)* dynamic fracture, viscoelasticity, crack		

20. ABSTRACT *(Continue on reverse side if necessary and identify by block number)*

Three areas of dynamic viscoelastic crack propagation are considered experimentally. To the extent that the gross mechanical properties of a material are viscoelastic, its fracture behavior should be influenced by rate effects (loading rates, crack speeds, etc.) and by temperature through the time-temperature relation.

Homalite 100 and a polyurethane, Solithane 113, chosen as model materials, are studied using the method of caustics and high speed photography.

DD $_{1\ JAN\ 73}^{FORM}$ 1473   EDITION OF 1 NOV 65 IS OBSOLETE

AD-A159 498

DTIC FILE COPY

85 09 11 027

The variation of the stress intensity factor and the velocity of a running crack are determined when initiated and driven by dynamic step loading on the faces of an initial semi-infinite crack in an infinite medium. Post-mortem analysis of the fracture surfaces and manipulation of parameters in the materials manufacturing process are utilized to illuminate the micromechanics of the fracture behavior, in particular as it relates to crack branching.

Accession For

NTIS GRA&I ☒
DTIC TAB ☐
Unannounced ☐
Justification

By
Distribution/
Availability Codes

| | Avail and/or |
| Dist | Special |

A-1

DTIC
COPY
INSPECTED
9

GRADUATE AERONAUTICAL LABORATORIES

CALIFORNIA INSTITUTE OF TECHNOLOGY
PASADENA, CALIFORNIA 91125

September 5, 1985

Defense Technical Information Center
Bldg. 5
Cameron Station
Alexandria, VA 22314

Contract No. ONR N00014-78-C-0634

To Whom It May Concern

Enclosed I am sending you a copy of the final report entitled
"Dynamic Fracture in Viscoelastic Solids."

Sincerely yours,

W.G. Knauss
Professor of Aeronautics
and Applied Mechanics

SM Report 85-14

Final Report to the

Office of Naval Research/Power Branch

on a Research Program on

DYNAMIC FRACTURE IN VISCOELASTIC SOLIDS

by

W.G. Knauss

June 1985

California Institute of Technology

Pasadena, CA 91125

TABLE OF CONTENTS

SUMMARY

The following synopses are the findings under this research project:

1. The method of optical caustics is extended for a steadily running crack in a viscoelastic medium and applied to the fracture testing of Homalite 100 at various temperatures. For further study of the crack tip stress field adiabatic conditions should, perhaps be incorporated in the formulation of the caustics.

2. The relation of the caustic creep function, index of refraction, and the history of mechanical deformation is obtained and compared with experimental results, and shows good aggreement.

3. The dependence of the crack speed on the stress intensity has been clarified for Homalite 100 at various temperatures. Specifically it is found, that at all temperatures considered the crack speed is, at best, insensitive if not independent of the stress intensity factor.

4. Fracture surfaces have been investigated microscopically and qualitative correlations among the roughness of the surface, stress intensity levels and temperature are observed.

5. In Solithane 113 the maximal crack speed takes on a higher fraction of the apparent Rayleigh wave speed than in any other polymeric solid examined to date.

1. INTRODUCTION

When one compares the progress made in understanding quasi-static fracture with that related to dynamic crack propagaion one is impressed with the wide range of engineering applications in which quasistatic fracture analyses have

proven useful. Speaking comparatively, much less understanding has been generated for dynamics related problems. No doubt it is primarily a matter of time before a body of knowledge on dynamic fracture has been developed that has a design oriented impact comparable to that which is now offered with respect to quasi-static fracture.

The problem of dynamic fracture in viscoelastic solids has enjoyed a proportionately still smaller degree of attention. This is in part due to the fact that

a. viscoelastic solids are relative newcomers on the engineering scene,

b. analytical treatment of dynamics problems is significantly more difficult than for purely elastic materials, and

c. interpretation of experimental work is severely limited by the lack of analytical understanding.

Because of this relative paucity of effort in dynamic fracture, there appears to have emerged in recent years several attempts to improve our empirical knowledge of dynamic fracture. However, these new developments are almost exclusively devoted to the fracture of rate insensitive materials. While experimentation proceeds with polymeric solids as test materials these polymers are chosen as metal substitutes primarily for reason of convenience; their viscoelastic behavior tends to be an undesirable inconvenience rather than a chosen characteristic.

This work was conducted to better define and predict the friability of strongly viscoelastic solids, and was oriented to better understand the effects of viscoelastic material behavior on the fracture process with particular attention devoted to comminution related problems. The motivation for this work derives from problems encountered in understanding safety limitations in handling the new high energy solid propellants (vulnerability) as well as the problem of

deflagration-to-detonation transition (DDT). Both phenomena depend potentially strongly on the rapid generation of large amounts of new (burning) surface such as is observed to occur usually in dynamic fracture processes. The time scale of dynamic fractures is typically in the high microsecond range (hundreds of μsec) and thus of the same order experienced in a motor DDT.

The basic interest here is to understand the conditions that lead to crack branching. For, if crack branching criteria can be established one would, in principle, be ale to estimate whether the dynamic stresses accompanying DDT could cause a rapid proliferation of crack surface via branching and thus feed the DDT process by offering a rapidly growing burning surface.

There are several important issues that are subordinate to this basic question:

(a) Wave propagation in viscoelastic solids: Simple problems of wave propagation involving viscoelastic material behaior are fairly well understood; so is the attenuation of propagating waves in simple geometries. However, in geometries involving cracks or even propagating cracks much less is known. It is hoped that work going on at this time at other institutions can usefully complement the present effort in the future. Of particular interest would be information on the crack tip strain field of a running crack.

(b) A problem similar and related to that just mentioned under (a) is the experimental identification of the crack tip stresses. To date this has been accomplished via optical caustics, although a slightly more laborious method, namely photoelasticity, could be employed. In either case the modification enforced by viscoelastic material behavior offers a major complication. We have assumed in part of our work employing caustics that a modicum of viscoelastic behavior does not materially affect the caustics, so that the crack tip stresses

are approximately determined by the caustics as interpreted via linear elasticity. for other parts of our investigation concerned with a stronger viscous material component that assumption is not justified and *ad hoc modifications need to be used.*

(c) Probably an important consideration in any explanation or theory for multiple crack branching is the microstructural response of the material at the crack tip. To date little attention has been paid to this fact, in part because virtually no information exists on its likely effect. As a consequence we report here some detailed, if initial, information on how the material responds as crack branching is approached.

(d) With this problem of microstructural effects is connected the general question of constitutive behavior of viscoelastic propellant materials under high rates of loading. That behavior is fairly well understood, as far as engineering accuracy is concerned as long as (strain) loading rates are below, say, 1000/sec. However, when rates 1000 times higher are involved time-temperature superposition is somewhat questionable without some further tests.

2. BRIEF REVIEW

In this work the fracture of viscoelastic polymers under dynamic loading is summarized. The loading condition is a step loading on the faces of a semi-infinite crack in an unbounded viscoelastic two-dimensional plane. The condition is simulated experimentally by applying on the crack faces electromagnetic forces induced by a square pulse of high electric current flowing in opposite directions through a doubled up thin copper strip; this strip, the legs of which are separated by a Mylar insulator 125 μm thick, is inserted into the crack of a large specimen plate. In order to control the intrinsic time scale of viscoelasticity, the temperature is changed through the use of the time-temperature shift

phenomenon. In these experiments, Homalite-100 is used at three different temperaures (60°C, 80°C, 100°C) under three different load levels. Solithane 113 (50/50) is also used in a similar fashion (0°C, −20°C, −40°C, −60°C).

The result of this study is basically divided into three parts. The first part is the characterization of the stress state near the crack tip, measuring the stress intensity factor K(t) as a function of time in the given load history. This is done experimentally by extending the method of caustics to viscoelastic materials. This extension is discussed later on in this report.

The second part concerns the process of fracture under the characterized stress state at the crack ip. This is investigated by relating the stress intensity factor and the corresponding velocity of the extending crack, and by observing the fracture surfaces microscopically. Together with the data of crack velocities at various temperatures, data for the initiation of a running crack are obtained. In addition it appears that the micromechanism of crack propagation is related to the stability of the crack front in the fracture surface plane; this behavior may be interpreted as producing discontinuous crack growth with the attendant generation of rough surfaces.

The third part concerns the behavior of crack branching. A possible mechanism of crack branching is suggested, which may explain the continuous energy release rate before and after branching. Observations seem to show that the branching is preceeded by the sequence of

i. division of crack front in the fracture surface plane,

ii. deviation of each of the new crack fronts from the original fracture surface plane due to crack path instability, and

iii. interaction of the deviated crack fronts which would cause further global branching depending on the stress state near the global crack front.

3. ELECTROMECHANICAL LOADING DEVICE

Our means of loading fracture panels has a number of advantages over mechanical loading systems. However, it has some disadvantages and steps were taken to improve the arrangement.

Briefly, the set-up is as follows: A long copper strip is doubled over on itself, an insulating strip of mylar is placed between the two halves of the copper and the amalgam is placed in a long slot in the fracture specimen (see Figure 1). When a current, supplied by a capacitor bank, is passed through the copper strip the Lorentz force generated pushes the halves of the copper strip away from each other and loads the panel. The system has a very fast rise time in the current pulse. Through appropriate use of impedance coils in the capacitor bank, the current pulse can be given virtually any shape (current vs. time), in particular a nearly square wave pulse. The energy supplied to the fracture panel is small in relation to the energy stored in the capacitor banks, so the current pulse is not a function of the deformation history of the panel and is thus highly repeatable. The timing interface between a high speed camera and the stress pulse is easily arranged since the systm is all electrical. With an appropriately sized specimen, an infinite plate can be similated for the duration of the test. This makes theoretical analyses much simpler.

Those are the advantages. Now for the problems and how they are being alleviated. Increasingly, we required higher and higher crack surface pressures. We also required this pressure over a larger and larger crack surface separation and over longer and longer time periods. As a result, three limitations came into play.

1. Despite the enormous energy which can be contained in a capacitor bank, it is not as easy to store a great deal of charge. The force generated in our copper loading strip is a function of the current. Clearly, we could not increase the force and the total time of application simultaneously.

2. The Lorentz force is a rather strong function of the strip separation.

3. The force on the copper strip, taken high enough, tended to tear the strip in half at the point where it bends back on itself.

All of these limitations could be overcome if one were willing to make a larger slot in the fracture panel. In the past, the copper strips have been made rather thin in order that the slot made in the specimen may be small and represent loading on a semi-infinite crack faces. Also, we had the width of the strip equal to the width of the plate. for increases in the slot thickness which are not too drastic, it would still approximately be loading along a semi-infinite crack. With this proviso it would seem reasonable to use a coiled copper strip configuration. The resulting increase in size and width act geometrically so that the force on the coil is less sensitive to crack separation than the single strip for these greater coil widths. However, it would become necessary to use a thick bar of backing material between the coil and fracture panel.

A model analytical problem of use is the following. Consider an infinitely long, solid copper strip separated from another strip of equal dimensions. If a current carried uniformly through the cross-section of the (assumed rectangular) copper passes in opposite directions in the wo strips, the separating force/length on each strip has the following mathematical form

$$\frac{d}{\sqrt{t\omega}} \equiv A, \quad \sqrt{\frac{t}{\omega}} \equiv B \tag{1}$$

$$\frac{\text{force/length}}{\frac{\mu_0}{4\pi} \frac{i^2}{(t\omega)^2} (t\omega)^{3/2}[2.100]} = F \tag{2}$$

with

$$F = \frac{1}{2.100} \left[\begin{array}{l} 2\pi B \\[2ex] \begin{array}{ll} +4\left[-\dfrac{1}{3B^3} + \dfrac{1}{B}(A + B)^2\right] & \\ & \tan^{-1}(B(A + B)) \\ -2\left[-\dfrac{1}{3B^3} + \dfrac{1}{B}(A)^2\right] & \tan^{-1}(BA) \\ & \tan^{-1}(B(A + 2B)) \\ -2\left[-\dfrac{1}{3B^3} + \dfrac{1}{B}(A + 2B)^2\right] & \end{array} \\[4ex] \begin{array}{ll} +2\left[-\dfrac{1}{B^2}(A + B) + \dfrac{1}{3}(A + B)^3\right] & \\ & \ln[B^2(A + B)^2 + 1] \\ -\left[-\dfrac{1}{B^2}(A) + \dfrac{1}{3}(A)^3\right] & \ln[B^2(A)^2 + 1] \\ & \ln[B^2(A + 2B)^2 + 1] \\ -\left[-\dfrac{1}{B^2}(A + 2B) + \dfrac{1}{3}(A + 2B)^3\right] & \end{array} \\[4ex] \begin{array}{ll} +2\left[-\dfrac{1}{3}(A + B)^3\right] & \\ & \ln[B^2(A + B)^2] \\ -\left[-\dfrac{1}{3}A^3\right] & \ln[B^2A^2] \\ & \ln[B^2(A + 2B)^2] \\ -\left[-\dfrac{1}{3}(A + 2B)^3\right] & \end{array} \end{array} \right] \tag{3}$$

where d is the separation distance between the nearest surfaces of the two strips, t is the thickness of each strip, ω the width, and i the current. F is normalized to attain a maximum value of 1. This occurs for $A = 0$ and $B = 0.695$. Figure 2 gives an indication of the variation of F with A and B.
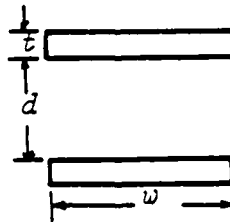
For a given d, $t\omega$ and $\frac{i}{t\omega}$, one might wish to pick $\frac{t}{\omega}$ to optimize on the force/length. In this case we have the implicit relation

$$
0 = \begin{cases}
(u^2-1)[2\tan^{-1}(u+v) -\tan^{-1}u -\tan^{-1}(u+2v)] \\
+ u\ln(u^2+1)[(u+2v)^2+1]/[(u+v)^2+1]^2 \\
+ v[(u+2v)^2+1]\ln[(u+2v)^2+1] -(u+2v)^2\ln[(u+2v)^2] \\
-v[(u+v)^2+1]\ln[(u+v)^2+1] -(u+v)^2\ln[(u+v)^2] \\
+2v^2[2\tan^{-1}(u+2v) -\pi/2 -\tan^{-1}(u+v)]
\end{cases}
\tag{4}
$$

where $u \equiv \frac{d}{\omega}$, and $v \equiv \frac{t}{\omega}$. Solving this equation numerically we have the resulting curve in Figure 3. This curve A vs. B is also indicated in Figure 2.

It is clear that there results a loss of loading capability if the copper strips are separated too much. If one deals with tough but compliant materials this loss of loading may reflect adversely on one's ability to generate fractures arbitrarily. To illustrate the difference between generating forces on materials of different compliance consider the following. From the analysis as outlined above one derives that the pressure applied to the crack faces as a function of strip separation is as shown in Figure 4. If one knew therefore what the instantaneous separation of the strips is, one could deduce the pressure pulse history to the crack surface. Accordingly the strip separation has been determined photographically in experiments. The result of this is shown in Figure5 and the time dependent evaluation in Figure6. Using Figures 5 and 6 one computes, therefore, the instantaneous pressure applied to the crack surfaces as given in Figure 7.

Note that for the compliant Solithane material, which corresponded to the properties at 20°C, there is a considerable loss of pressure at times roughly beyond 50-60 μs. The arrangement therefore produces a load history that is more appropriately represented by a pressure pulse on the order of 60 μs

roughly with a ramp type loading and ramp type unloading. Drawing again for a moment on purely elastic results, as shown in the left inset in Figure 8, we can, by a superposition of that result in terms of loading and delayed unloading of the same type, compute the stress intensity factor for a pressure pulse as indicated in the right inset in that figure. Thus while a relatively stiff material, such as Homalite 100 at room temperature would produce significant stress intensities for times on the order of a 100 to 150 μs the softer Solithane type of material at least for tmperatures around room conditions would produce stress intensities that are approximately 25% of that produced in Homalite 100, although at short times up to approximately 50 μs the same kind of stress intensities would result.

We see thus that with compliant materials it is not easy to generate high pressure pulses with electromagnetic means, although the precision with which experimental synchronization can be achieved is superior to any other way of stress wave loading. There are, however ways of enlarging the pressure transmission through optimizing the shape of the copper strip-driver as indicated above. This optimization has not (yet) been attempted in the laboratory.

4. DETERMINATION OF THE STRESS INTENSITY BY THE METHOD OF CAUSTICS

In experimental stress analyses relating to static or dynamic cracks, there are generally two techniques that have evolved during the past decades to measure stress intensity factors. The most recent development in that direction has been the method of caustics which is the one that is adopted in this work. The somewhat older and more classical method is based on photoelasticity. Either method has been employed to date primarily to elastic materials. This is unequivocally true with respect to dynamic problems. It turns out that the photoelastic method has certain disadvantages for our investigation: Most important

among these restrictions is that the Homalite 100 material with which we were working in a part of this investigation, was used in relatively thin sheets (3/16 inch thick) and the fringe count was not sufficiently high to give a reasonable number of fringes in these tests. There are a number of fringe multiplication techniques available; however, they require a large amount of light which is not available in our set-up but which is required for the very high speed photography used here.

Apart from these limitations arising from the specimen size and from the experimental equipment it turns out that the fringe interpretation - through fitting an analytical expression in a least square fit - has no greater accuracy than the limitations inherent in the caustic method. Beyond this comparison it turns out that the caustic method was well suited to our optical setup allowing sufficient passage of light in a single pass from the laser light source to expose the film during the 20 nano second exposure required for stop action at 100,000 frames/sec as employed in these tests. Moreover, in some of our tests (on Solithane 113) the rigidity of the test material is relatively small. As a consequence somewhat larger than "normal" deformations occur which cause a relatively large deflection of the light beam. As a result, it is difficult to capture all this information with a reasonably sized lense. In contrast the caustic method exhibits many fewer difficulties and is relatively simple to apply. For this reason we extended the computations underlying the shape of the caustic in elastic materials to viscoelastic fracture.

For reference purposes consider the optical set-up shown in Figure 9. Denote a generic point in the crack tip vicinity by $\underline{x}$ and consider a light ray passing through this point $\underline{x}$ in the loaded specimen. In the image plane the ray strikes the corresponding point $\bar{x}$ so that we have the transformation

$$\overline{x}' = \underline{x} + \overline{\omega}(\underline{x}, t) \tag{5}$$

where we denote by $\overline{\omega}$ the deflection vector due to the stress state near the crack tip. This deflection vector can be expressed as

$$\overline{\omega}(\underline{x}, t) = z_o \, \nabla \, \Delta s(\underline{x}, t) \tag{6}$$

where z_o is the distance between the stress specimen midplane and the image plane and Δs is the change of the effective optical path length

$$\Delta s = d_o C^* \{ \sigma_I + \sigma_{II} \pm \lambda (\sigma_I - \sigma_{II}) \} . \tag{7}$$

This change of the optical path length depends on the principal stresses at the point $\underline{x}$ on the specimen thickness d_o and on a constant C (a shadow optical constant). If the material is optically anisotropic a parameter λ will enter into the relation between the optical path length change and the state of stress. For optically isotropic materials this constant or anisotropy function is zero. For a viscoelastic material the optical path length is a function of the stress history. Expressed mathematically for a linearly viscoelastic system the path length difference is C(t). For isotropic linearly viscoelastic material we have, therefore, instead of equation (7)

$$\Delta s = d_o C^* \sigma \tag{8}$$

where we have written σ for the first stress invariant (sum of the principal stresses) and allowed for isotropic behavior only. Using these stress representations in the immediate vicinity of the crack tip for which, with mode I stress intensity factor K_I, we have

$$\sigma = K_I \sqrt{\frac{2}{\pi r}} \cos \frac{\vartheta}{2} + a \tag{9}$$

where $r = \sqrt{x_1^2 + x_2^2}$, $\vartheta = \tan^{-1} \frac{x_2}{x_1}$, and "a" is a constant. Making use of equations (5), (6), (8), and (9) there results

$$J = \frac{\partial(x_1', x_2')}{\partial(x_1, x_2)} = 0$$

one obtains for the shape equation of caustics the relation

$$r = (\frac{3z_0 d_0}{2\sqrt{2\pi}} C^* K_I)^{2/5}$$

or

$$K_I = \frac{2\sqrt{2\pi}}{3z_0 d_0} | C^{-1} | {}^* r^{5/2} \qquad (11)$$

This equation is, strictly speaking, true only for a stationary crack and it is therefore used for the variation in the stress intensity factor of a stationary crack (see below). We now turn to the measurement of the shadow optical function $C(t)$. Clearly the function $C(t)$ is of primary importance in the experimental evaluation of stress intensity factors in viscoelastic materials.

4.1 The Caustic for a Stationary Crack in a Viscoelastic Material

Equation (11) may be rewritten upon using equation (5), (6), and (8) to yield

$$K_I = \frac{\sqrt{2\pi}}{3 f^{5/2} z_0 d_0} | C^{-1} | {}^* D_0^{5/2} \qquad (12)$$

In this latter form D_0 denotes the diameter across the caustic in the y-direction; f is a constant for a linearly elastic material and for small angular deflection of the light by the specimen. As will be seen later, for the dynamic viscoelastic case as well, f may be considered a constant. The shadow optical function C is composed of two contributions. One arises from the change of the index of refraction, (denote this contribution by A) and by the lense like deformation of the viscoelastic sheet and; this contribution is given by $(n-1) \frac{\nu}{E(t)}$ so that C may be defined as

$$C = A - (n-1)\frac{\nu}{E} \tag{13}$$

Let us assume now that the contribution (optical relaxation) to a change in the index of refraction is small and proportional to mechanical relaxation, say, $\varepsilon \cdot \frac{\nu}{E}$, then C is given only by the rigidity contribution

$$C = (1 - n + \varepsilon)\frac{\nu}{E} \tag{14}$$

which allows us to write (12) as

$$(1 - n + \varepsilon)\frac{3z_o d_o}{\sqrt{2\pi}}(\frac{\nu}{E^*}K_I) = \{\frac{D_o}{f}\}^{5/2} .$$

Clearly this equation indicates that if a stress intensity factor of known magnitude acts at the tip of the crack, then the caustic diameter D_o should grow in conformity with the shadow optic function C(t). Moreover, this shadow optic function should be directly proportional to the creep compliance - or at worst a convolution of a creep compliance and Poisson's ratio - in accordance with equation (14).

In order to test out this relation it is appropriate to make use of the viscoelastic properties of Solithane 113 and devise a geometry with a non-propagating crack. Such a geometries is given by a large sheet with a central crack perforation. The stress intensity factor for this problem remains constant if a step function as the far field stress is applied. In Figure 10 a and b we show a sequence of time exposures of a caustic at the tips of such a crack in Solithane 113. These particular figures were taken at -10 and $-15°C$; clearly the diameter of the caustic is seen to grow with time after load application. This type of data is then obtained at three different temperaures and the results suitably normalized are shown in Figure 11. Also shown in that figure is the reciprocal Young's relaxation modulus normalized by its value at infinite time - that is, by its

rubbery modulus. This function is taken as an approximation to the creep compliance in uniaxial tension. It is seen that the comparison of the analytical estimate is quite reasonable with the data derived from tests. The data derived from these three temperatures has been superposed according to the time temperature shift phenomenon making use of the shift factor which has been determined previously for Solithane 113.

In Figure 12 the shadow optical function for Homalite 100 is given reduced to a temperature of 60°C. This curve is the result of tests at temperatures of 60, 80, and 100°C with an estimated scatter band as indicated by the error bar.

Both curves for the shadow optical functions are basic input into the experimental determination of the stress intensity factor for running cracks: The shape and size of the caustic involves a convolution of this property with the deformation history at the tip of the moving crack tip. We proceed to discuss now this analytical problem.

4.2 Analytical Determination of the Caustics for a Crack Moving in a Viscoelastic Solid

We need to recall that analyses of the dynamic stress intensity factor for a moving crack tip are usually formulated so that the state variables such as stress, strain, etc., are expressed in terms of a position vector $\underline{x}$ which has its origin a the running crack tip. In contrast the shadow optic function $C(t)$ is a material property and therefore the appropriate convolution "*" has to be applied with respect to a fixed material point $\underline{X}$ in equation (7). Accordingly the expression for the optical path length which is commensurate with equation (10) is given by

$$\Delta s = d_o \int_{-\infty}^{t} C(t - \tau) \left(-v \frac{\partial \sigma}{\partial x_1} + \frac{\partial \sigma}{\partial \tau}\right) \underline{x} d\tau \qquad (15)$$

where v is the velocity of the crack tip and it is assumed that the crack pro-

pagates in the positive x_1 direction.

Let us now turn to consider an approximation for the caustic in a viscoelastic material arising from a crack tip moving through a two-dimensional geometry. We consider this in the context of a problem of plane stress. Drawing on the results with the stationary crack in which case this stress at the crack tip could be written as a product function of a time dependent stress intensity factor and a function representing this spatial distribution of the stresses, we write tentatively for the dynamic case

$$\sigma[\underline{x}(\underline{X},t),t] \approx K(t)f[\underline{x}(\underline{X},t);v] + a . \tag{16}$$

Although there exists an explicit form for the function $f(\underline{x};v)$ for the case of dynamically moving cracks in an elastic material this function is not available for the viscoelastic material. However, in order to arrive at an adequate estimate we note that the speed of cracks in viscoelastic materials tends to be relatively low. This observation allows us to disregard dynamic effects in this stress distribution so that we may make use of the quasi-static stress distribution as an approximation. In accordance with equation (9) we use

$$f(\underline{x}) = \{ \frac{x_1 + (x_1^2 + x_2^2)^{1/2}}{\pi(x_1^2 + x_2^2)} \}^{1/2} \tag{17}$$

It is a general observation that for crack propagation velocities less than about half the Rayleigh surface wave speed, the error due to the use of quasi-static behavior is within the range of experimental error for the elastodynamic crack problem. Making use of this assumption. we obtain for the deflection vector of the light rays in passing through the deformed crack tip area. via equations (6), (9), (15), and (17) as

$$\overline{\omega}[\underline{x}(\underline{X},t),t] = d_0 z_0 \nabla [\int_{-\infty}^{t} C(t-\xi)\{-K(\xi)v(\xi)\frac{\partial f}{\partial x_1}[\underline{x}(\underline{X},\xi)] + \frac{\partial K(\xi)}{\partial \xi}f[\underline{x}(\underline{X},\xi)]\}d\xi] \tag{18}$$

Upon integrating this by parts we obtain the result

$$\varpi[\underline{x}(\underline{X},t),t] = d_0 z_0 \{K(t)C(o)\nabla\ f[\underline{x}(\underline{X},t)] + \int_{t_0}^{t} C'(t-\xi)K(\xi)\ \nabla\ f[\underline{x}(\underline{X},\xi)]d\xi\} \qquad (19)$$

where t_0 denotes the time when the loading of $K(t)$ begins and $C'(t) = \dfrac{dC}{dt}$.

In order to compute the shape of the caustic we have to make use again of the condition that the Jacobian

$$J = \frac{\partial(x_1,x_2)}{\partial(x_1,x_2)} = 0$$

of the transformation represented by equations (5) and (19) vanishes. However, we are not really interested in the shape of the caustic for a given history of the stress intensity factor. Rather, we are only interested in the measurement of the stress intensity factor as a function of velocity and time. It indeed turns out from experiments described later that the shape of the caustic for a crack running in a viscoelastic material is not much different at all from that of the stationary crack for the velocities encountered in our experiments. In order to determine the radius of the initial curve it is therefore not necessary to compute the total shape of the caustic; rather it is sufficient to compute this radius r_0 by using the condition that on the crack axis.

$$|\ \frac{\partial x_1}{\partial x_1}\ |_{x_2=0} = 0\ . \qquad (20)$$

Let us make the further assumption that the stress intensity factor varies slowly. This is actually a condition found in our experiments. Then $\dfrac{\partial K}{\partial t} = 0$ and the second term in equation (18) is assumed to be negligibly small due to the structure of the function $f[\underline{x}(\underline{X},\tau)]$. If in addition the acceleration of the crack is small we can obtain from equation (18) the deflection vector of the light rays as

$$\omega_1[x(X,t),t] = -d_o z_o K(t) v(t) \int_{-\infty}^{t} C(t-\xi) \frac{\partial^2 f}{\partial x_1^2} [x(X,\xi)] d\xi \tag{21}$$

$$x_1(X,\xi) = x_1(X,t) + (t-\xi)v_o \tag{22}$$

and v_o denotes the speed of the crack. Then, the condition

$$\frac{\partial x_1'}{\partial x_1} \Big|_{x_2=0} = 0 \quad \left(\text{or} \quad \frac{\partial w_1}{\partial x_1} \Big|_{x_2=0} = -1 \right)$$

renders the stress intensity factor

$$K = \frac{4\sqrt{2\pi}}{15 d_o z_o \int_{o}^{\infty} \frac{|C(\chi/v_o)|}{(r_o + \chi)^{7/2}} d\chi} . \tag{23}$$

Let us now examine the limit expressions for the stress intensity factor in equation (23) namely for the cases of vanishing and for infinite crack propagation velocity v_o. One has then

$$K = \frac{2\sqrt{2\pi}}{3 z_o d_o |C(\infty)|} r_o^{5/2} \quad v_o \to 0$$

$$K = \frac{2\sqrt{2\pi}}{3 z_o d_o |C(0)|} r_o^{5/2} \quad v_o \to \infty . \tag{24}$$

These expressions correspond to the elastic expressions except that the optical constants are replaced by $C(\infty)$ and $C(o)$, respectively. In general, the function $C(\xi/v_o)$ is the function shown in Figures 11 and 12 for Solithane 113 and Homalite 100, respectively.

In any experiment the diameter of the caustic along the line normal to the plane of crack propagation is used as a definition for the size of the caustic. This diameter D is related to the radius of the initial curve by $r_o = mD$. For the case of parallel incident light, this constant is, for a stationary crack, equal to $m = 1/3 \cdot 17$. We have now estimated the size of the caustic and thus provided the tool to measure the stress intensity factor instantaneously for a crack pro-

pagating in a viscoelastic material.

Because the value of r_0 cannot be determined directly from experimental records one must generate both the caustic and the initial curve mathematically. From the proper caustic as determined from the experiments one then deduces the appropriate value of the initial curve radius r_0. In Figure 13 caustics and associated initial curves are shown at different temperatures and different velocities. These curves are excerpts of complete ray plots, an example of which is shown in the lower portion of Figure 14.

It is of interest to note that ahead of the moving crack tip the caustic and the initial curve have very nearly the shape of those encountered with linearly elastic materials. However, it is at low velocities and at elevated temperatures that the "wake", i.e. the portion behind the moving tip, is noticeably different; this is so because of the viscoelastic rather than elastic unloading process.

Further evaluations and results along these lines are still under investigation in connection with a continuing but separate program. These results are in the process of being written up for publication and copies of these, together with the appropriate acknowledgement will be forwarded as soon as the papers are completed.

5. RELATION BETWEEN STRESS INTENSITY FACTOR AND CRACK SPEED

Since this program ran parallel to another one which was concerned with the dynamic fracture of brittle solids certain features seemed worthy of particular attention. Specifically it had been found in that program that there was a decided lack of correlation, to say the least, between the instantaneous stress intensity factor and the instantaneous crack speed. We examine this feature next.

In Figure 15a we show the variation of stress intensity factors after the crack has started to propagate. In this type of loading the stress intensity level is controlled by the running crack initiation time as well as by the strength of pressure applied on the crack faces. The general behavior of the initial drop in the stress intensity factor due to dynamic reduction (unloading) factors is similar to that in elastic materials. After dropping to a minimum the stress intensity factor increases again due to the loading history of the test. However, we note that in every case the velocity of the crack remains constant, within the experimental error, which is on the order of 2% with respect to the velocity determination.

These results are plotted for $K_I - v$ relations in Figure 15b and compared to those obtained by other investigators at room temperature. These data are normalized and also compared in Figure 15c to the analytical prediction for an elastic solid fracturing with expenditure of a constant fracture energy. It shows that a temperature increase reduces the speed of crack propagation for the given stress intensity level: this behavior is opposite in trend to that of low speed (creep) crack growth. This dependence is shown graphically in Figure 16 for Homalite 100 and in Figure 17 for Solithane 113. One notes that for both data sets the temperature range explored falls below the glass transition temperature, that of Homalite 100 being about 100°C. The retardation as a result of increased viscous effects as the glass transition is approached is thus real.

6. THE CRACK SPEED IN SOLITHANE 113 RELATIVE TO THE RAYLEIGH WAVE SPEED

Measurements of the crack speed in Solithane 113 provided the somewhat surprising result that in this material the crack speed can take on a higher fraction of the Rayleigh wave speed than in other solids like Homalite 100. If the energy required to create new surfaces is assumed to be a constant, the elasto-

dynamic theory predicts that the maximum velocity with which a crack may propagate is limited by the Rayleigh surface wave velocity, C_r. In most polymeric materials, the maximum velocity with which cracks have been observed to propagate is typically on the order of 0.5 C_r. But in Solithane 113, the maximum velocity seems to be a much higher fraction of C_r. At this time, we have no precise data on the value of C_r for Solithane, but base our conclusions on reasonable estimates of the Rayleigh wave velocity. Swanson[1] estimates the glassy value of C_r to be 350 m/sec. Gupta and Murri[2] measured the shear wave velocity in Solithane under pressures of 2.1 kbar to 14.3 kbar and obtained values in the range of 590 m/sec to 930 m/sec. Since in our tests, the applied loads were in the range of 0.5 kbar, if we use the lower end of the wave speeds, and estimate the Rayleigh wave velocity as 90% of the shear wave velocity, then we get C_r to be 530 m/sec. If we assume a glassy modulus of elasticity, appropriate to our loading rate and temperature to be 690 MPa, we get an estimate of C_r of 500 m/sec. We might consider these values as a possible range of Rayleigh wave velocities. A high estimate of the Rayleigh wave speed, calculated from Schnur's[3] value for the modulus of elasticity appropriate to the GHz response is in the range of 1000 m/sec. Since the loading system used in the present tests generates loads with a frequency content in the range of 20 kHz,[4] the above estimate may not be particularly applicable to the present case. From experimental measurements, we obtain crack velocities in the range of 400 m/sec. From the estimates we have reason to believe that cracks propagate at much higher fraction of C_r in Solithane than in other polymers. This could also point out to a significant

1. Swanson, S.R., "Crack Velocity Measurements in Solithane 113," Technical Report to ONR Contract # N00014-80-C-0156 (1982), p. 7.

2. Gupta, Y.M. and Murri, W.J., "Response of a Plain and Filled Elastomer (Solithane 113) to High Strain Rate Compression, Shear and Tensile Loading," Technical Report to ONR, SRI Project PYU 7802 (1981).

3. Schnur, J.M., NRL Memorandum Report 4323 (1980), p. 34.

4. Gupta, M. and Knauss, W.G., "Dynamic Fracture in Viscoelastic Solids," First Annual Report of Office of Naval Research Contract # N00014-78-C-0634, California Institute of Technology, 1979.

difference in the process of crack propagation in solithane and an examination of the fracture surface reinforces this view.

7. CRACK BRANCHING RESULTS

In solid propellant rocket motors, the rapid generation of new burning surfaces due to crack branching leads to a transition from the desirable deflagration to a destructive detonation. In order to prevent such a transition, one needs first to study the underlying mechanism that leads to crack branching. In a parallel research effort supported by the National Science Foundation, the mechanics of branching of brittle elastic materials has been investigated.[5] One of the goals of the present investigation was to explore the mechanism of crack branching in viscoelastic materials, with and without filler particles and also with voids. In this section, we present some of the results obtained with regard to crack branching in Solithane 113.

Solithane 113 is a very tough material and at room temperatures (i.e. aove the glass transition temperature in Solithane), it was not possible to propagate cracks rapidly. It was, however, possible to generate high speed cracks at low temperatures ($-20°C$ to $-90°C$). The crack propagation tests indicated that the energy required to branch cracks might indeed be very high and pointed to a limitation in the loading device. It was possible to have reflected waves interact with the propagating crack tip. since these waves are tensile in nature, (the compressive outgoing waves having been reflected from a stress free surface) the stress intensity factor at the crack tip increases and induces branching. Even though this is a little different from spontaneous branching, it provides us with information on crack branching. By comparing with the results from brittle materials, we gain some understanding of the branching process.

5. Ravi-Chandar, K., Ph.D. Thesis, California Institute of Technology, 1982.

Figure 18 shows Solithane specimens fractured at various load levels. The temperature and load levels are indicated in the figure. The optical quality of the specimens was poor and hence no quantitative data could be obtained from the caustics. However, an examination of the fracture pattern and surface structure did yield information on branching. On a macroscopic scale, crack propagation and branching in Solithane appear to be essentially similar to brittle fracture in, say, Homalite 100, supporting our belief that the viscous behavior may be separable from the fracture aspect. The first and fourth specimens had inserts with glass bead filler particles. Comparing specimens 3 and 4, we see no macroscopic effect of these in the overall fracture pattern. (Both specimens 3 and 4 have section lines necessitated for microscopic fracture surface examination.) The dark pathes and the secondary fractures are due to the copper strip breaking apart and establishing an arc. The microscopic nature of the fracture surface is discussed in the next section.

8. FRACTURE SURFACE MORPHOLOGY

The process of crack propagation, while modelled in the usual continuum sense, is essentially a three-dimensional problem of breaking of bonds at the atomic level. Although detailed computation of the fracture behavior from such an atomistic viewpoint is rather complicated one can understand much about the fracture processes by examining the microscopic nature of fracture. In this section, we deal with the post-mortem microscopic observations of the fracture surface. We will contrast the dynamically generated fracture surface, first with quasistatically generated surface in Solithane and secondly with dynamically generated fracture surface in other polymeric materials.

Figure 19 shows a quasi-statically generated fracture surface. Comparing the dynamically generated surface shown in Figure 19, it is seen that the former is

almost featureless, but the latter has a number of conic markings. These markings are caused by the crack front running into microcracks *that grow ahead of the crack front or microcracks running into one another*. If the microcrack growth speed is the same as that of the main crack, neglecting the interaction of the stress fields, one can show that the conic markings are parabolic.[6] This is confirmed by analysing the shape of the fracture surface markings such as the one shown in Figure 20. From the size of the parabolas, which have a focal length in the range of 30 microns, we see that the time for their emergence is very short (75 nsec if the crack speed is 400 m.sec) and insufficient for communicating with other flaws unless they are very close to each other. This would explain the absence of significant interaction of the stress fields. When microcracks run into one another, the resulting pattern is hyperbolic and can be explained by the following simple model. Consider a flaw at $(x,y) = (-c,o)$ starting to grow with a velocity u at time $t=0$ and another flaw at (c,o) growing with the same velocity u, but at time $t=t_o$. This situation is illustrated below. The equations for the growth of the two flaws are:

$$(x + c)^2 + y^2 = u^2 t^2$$

$$(x - c)^2 + y^2 = u^2(t - t_o^2)$$

The contour over which the two flaws run into each other is obtained by eliminating t between the two equations and is given by

$$\frac{x^2}{(\frac{ut_o}{2})^2} - \frac{y^2}{[c^2 - (\frac{ut_o}{2})^2]} = 1 \tag{25}$$

which is a hyperbola. Such hyperbolic markings we observed on the fracture surface and a typical one is shown in Figure 21. At high magnifications, it is possible to identify a number of flaws at the foci of these parabolas as in Figure 20.

6. Feltner, C.E., University of Illinois T&AM Report No. 224 (1962).
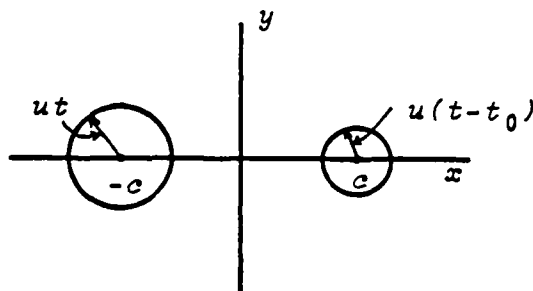
The fracture surface roughness appears to increase with increasing stress intensity factor, analogous to the behavior in brittle materials.

Let us now compare the microscopic detail of the fracture surface in Solithane with Plexiglas (Figure 19) and Homalite (Figure 19). In all three materials we observe parabolic markings, but the density of such markings differs considerably. In Homalite, relatively few distinct parabolas are seen, in Plexiglas more distinct parabolas are seen and in Solithane, the whole plane appears tiled with parabolic markings. The sizes of the parabolic markings also differ considerably. This points to a fundamental difference in the nature of the fracture process in these materials. The presence of a large number of parabolas indicates that a number of microcracks are formed ahead of the main crack front and crack propagation takes place essentially by a coalescence of these micro cracks.

We now turn to the effect of voids and filler particles on the fracture surface. Large voids and filler particles were introduced in the Solithane specimens using the techniques described in the Appendix. There was no apparent macroscopic effect of these voids and glass bead filler particles on the crack propagation process. However, there appeared to be some local effects due to the voids and beads. Figure 22 shows the fracture surface from a specimen in which a

number of large voids were present. Figure 23 shows the fracture surface in a specimen that contained glass bead filler particles. The direction of the arrow indicates the direction of crack propagation. The lower left hand side (in the photograph) is a region with no filler particles and the opposite side has a number of glass beads. Voids or filler particles which are slightly out of the plane of the approaching crack front cause the crack to diverge locally by amounts which are on the same order of magnitude as the size of the inclusion. In other words, *inclusions sufficiently removed from the crack plane have no apparent effect on the crack surface character or on the crack propagation and branching behavior.*
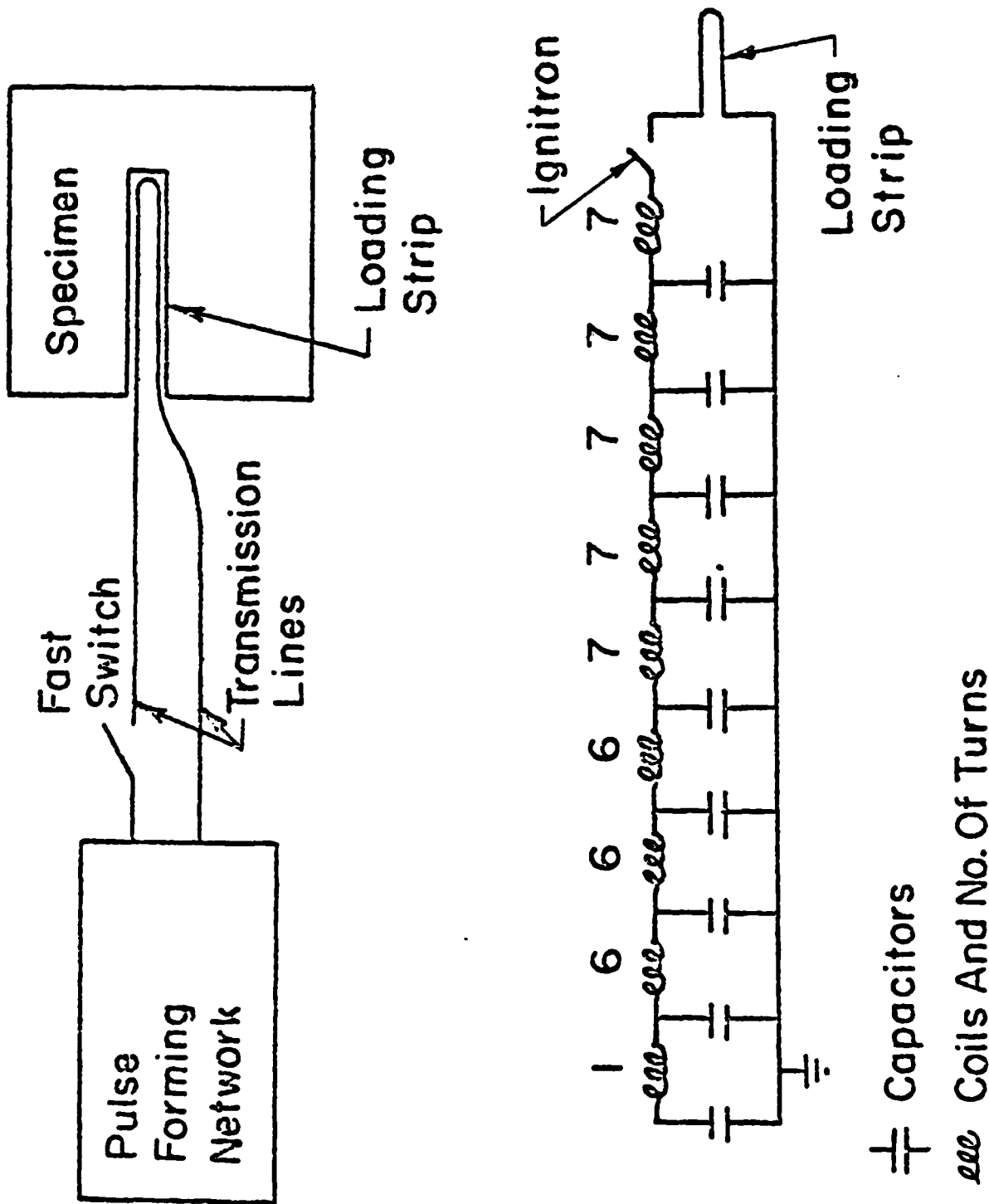
Figure 1. Schematic of the dynamic loading device.
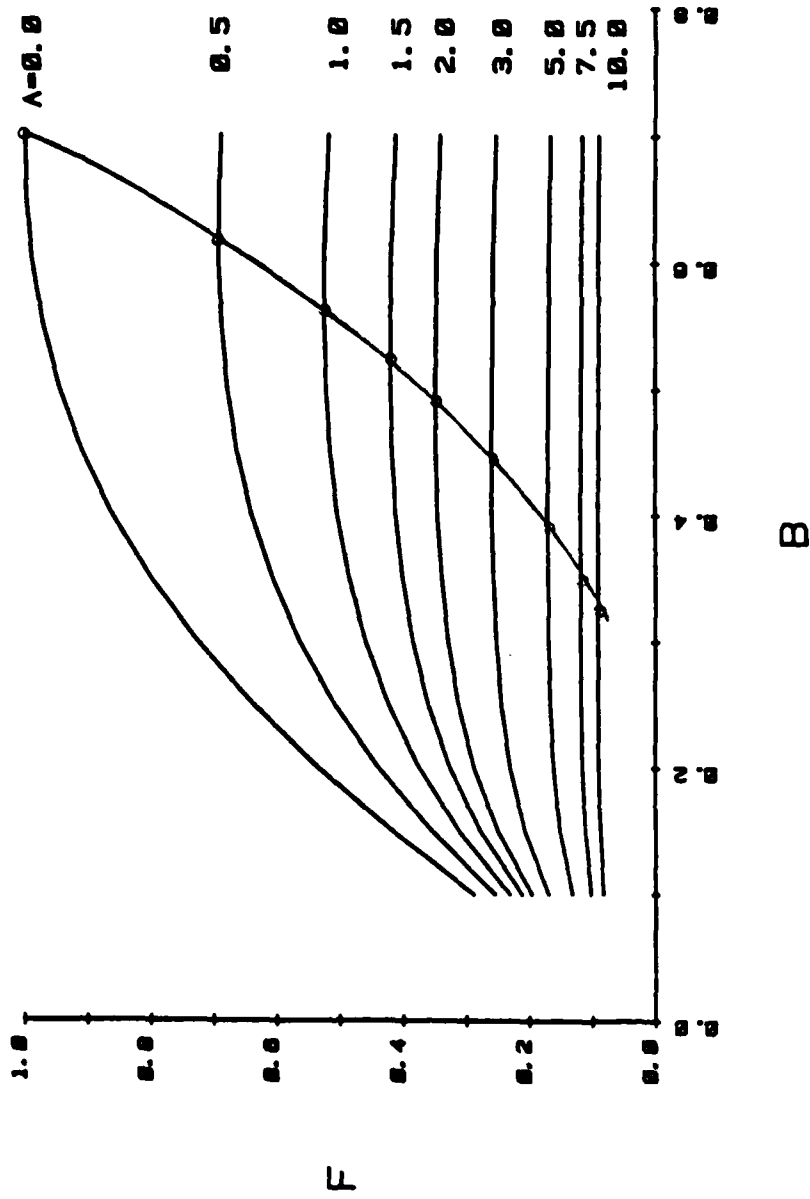
Figure 2. Geometric effects on the electromagnetic loading device.
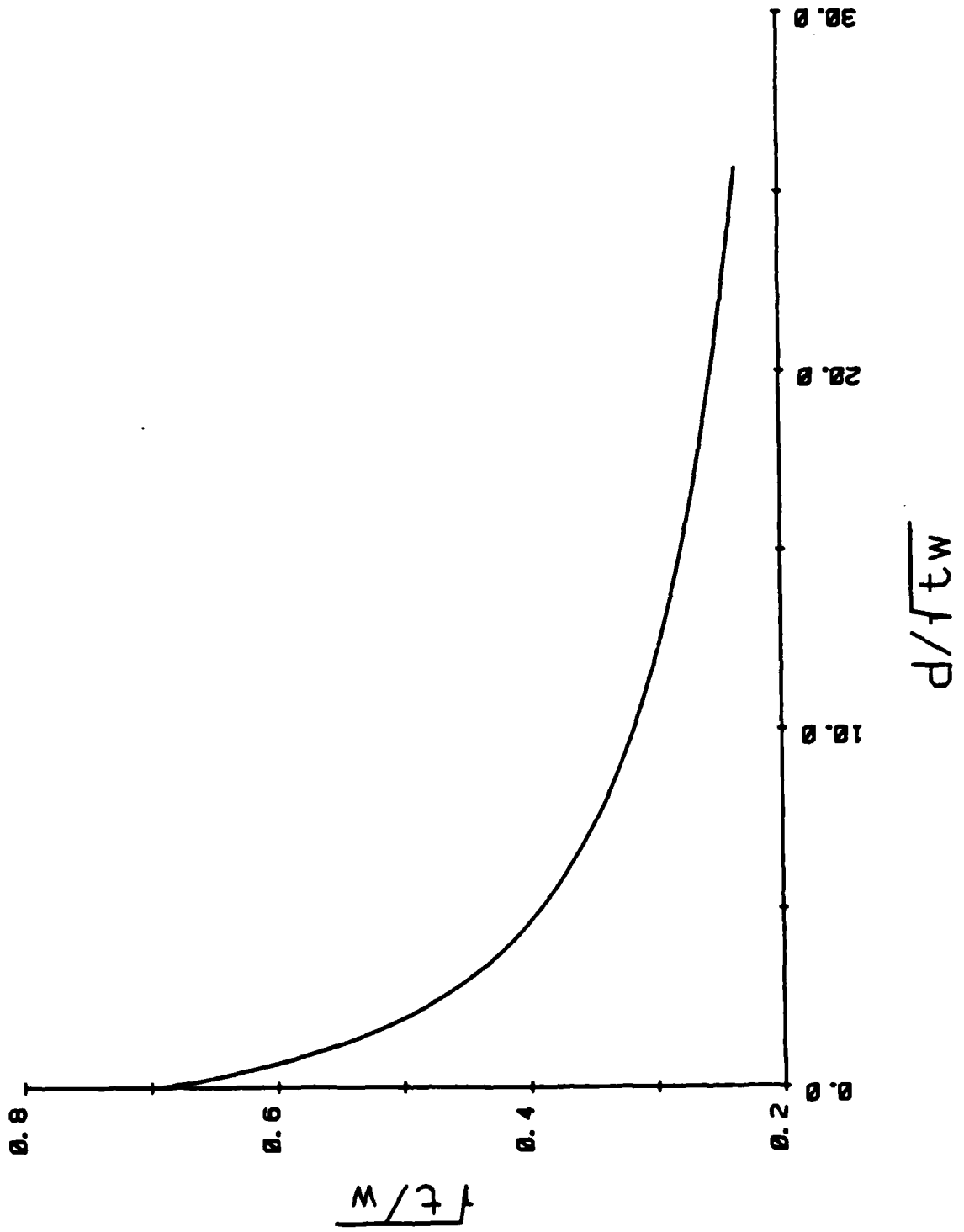
Figure 3.   Optimization of F with respect to t/w.
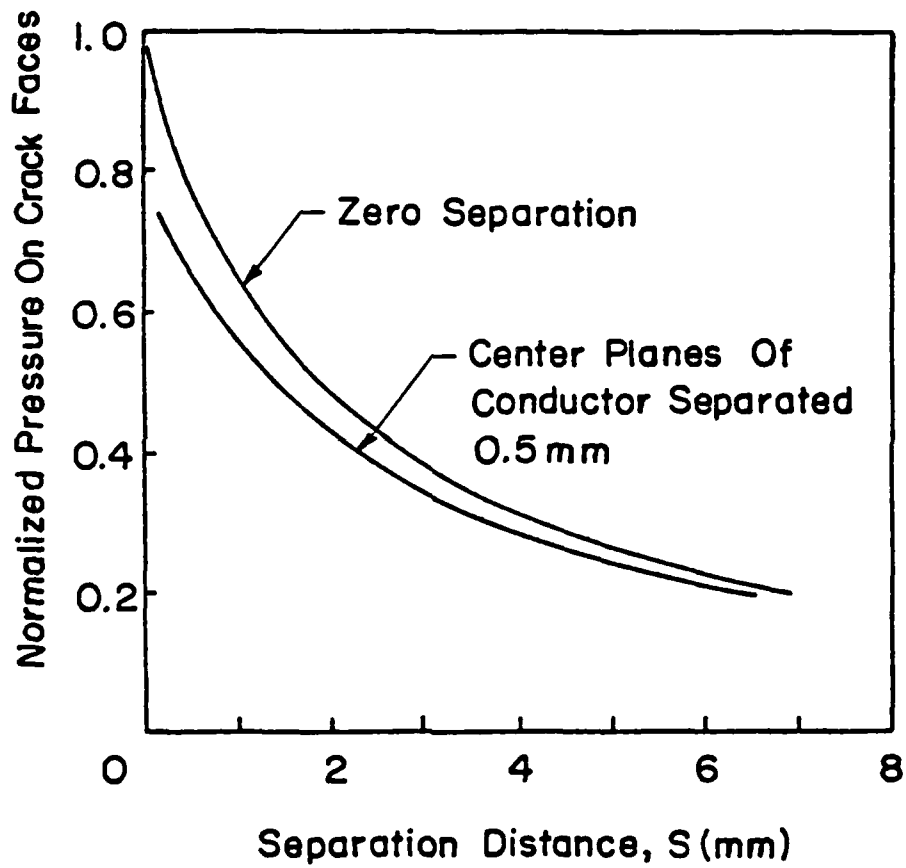
Figure 4.   Pressure produced on crack faces as a function of strip separation.
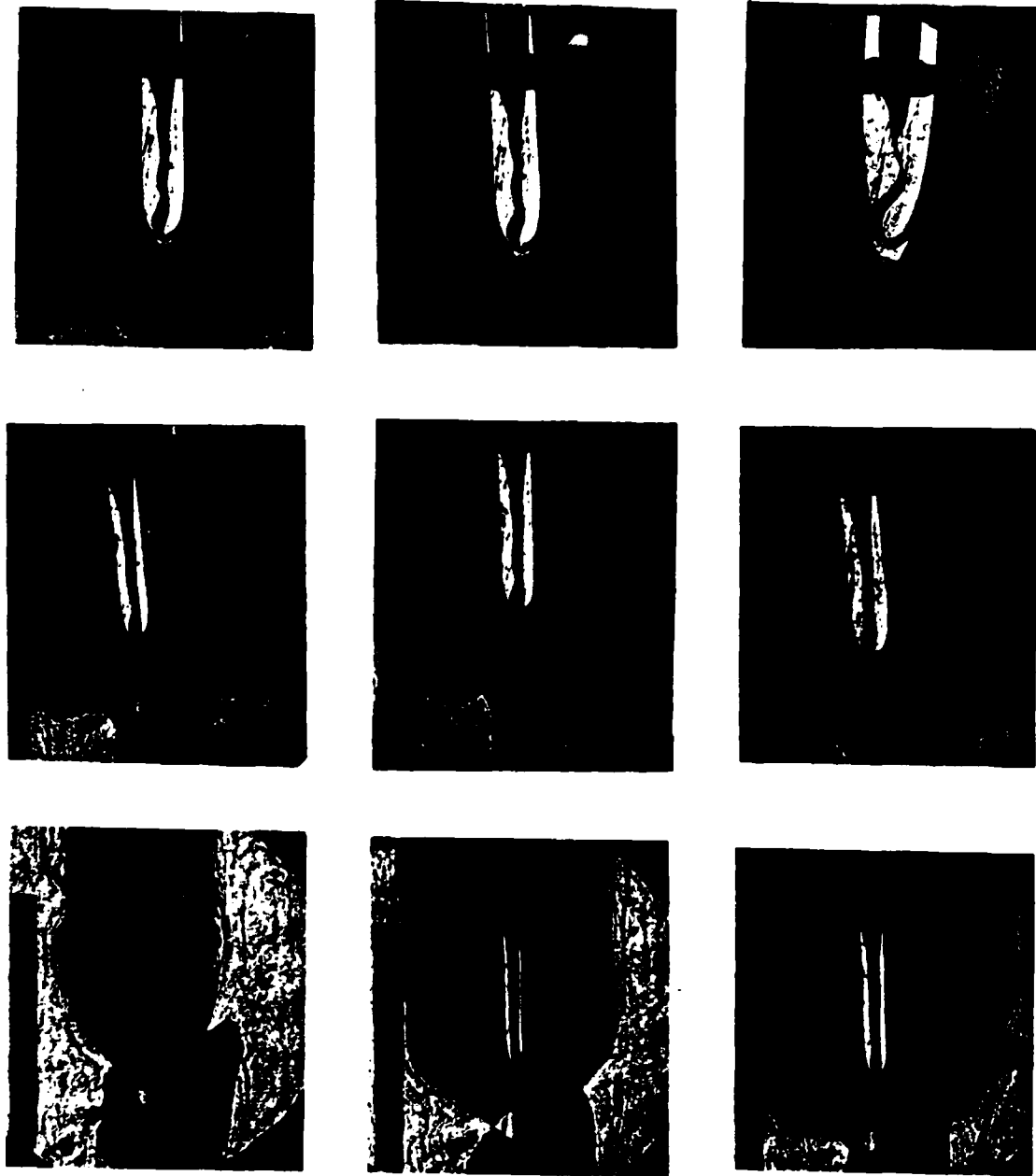
Figure 5. Time dependence of crack opening displacement in Solithane 113 at 20°C.
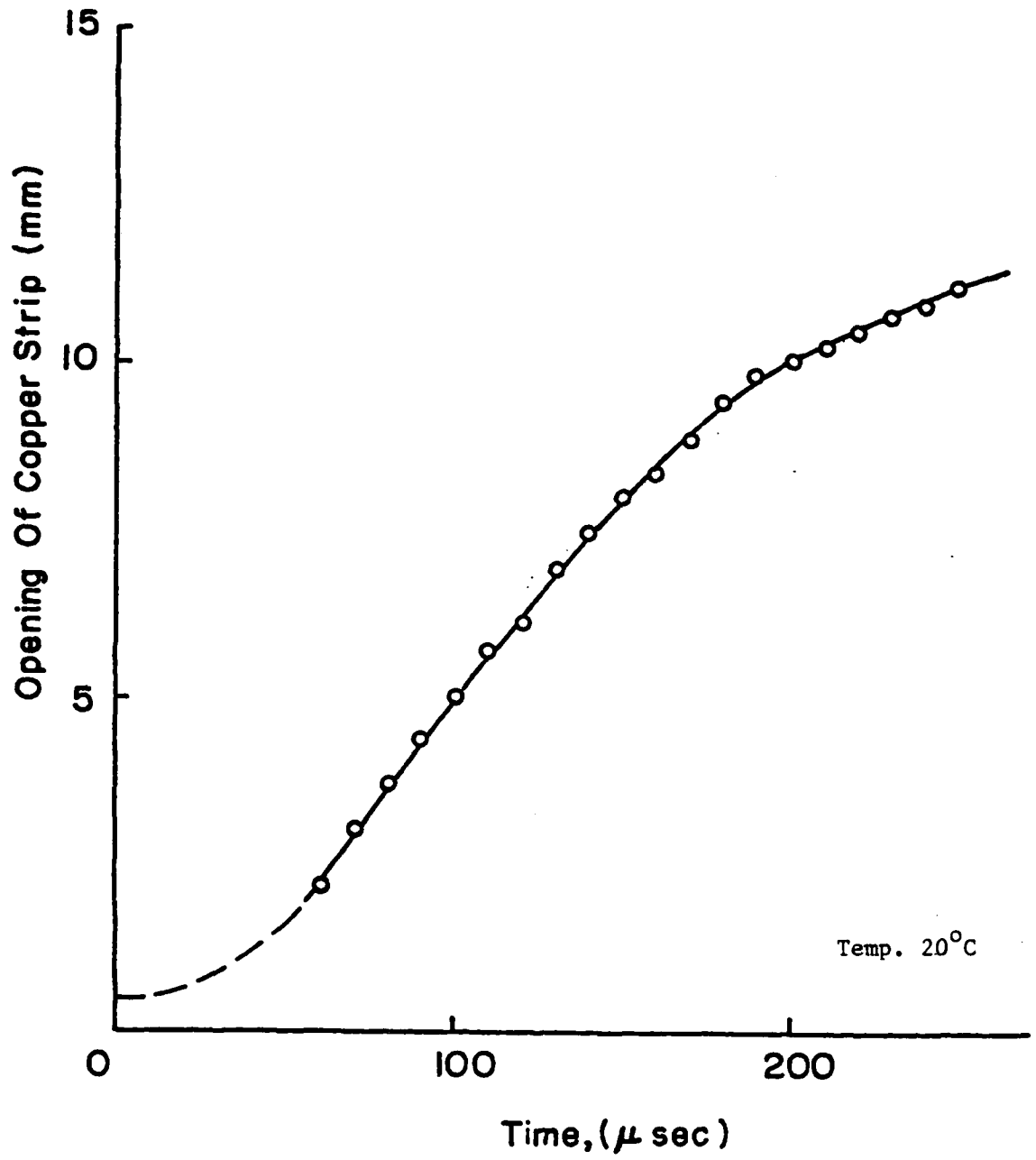
Figure 6. Crack opening displacement vs. time.
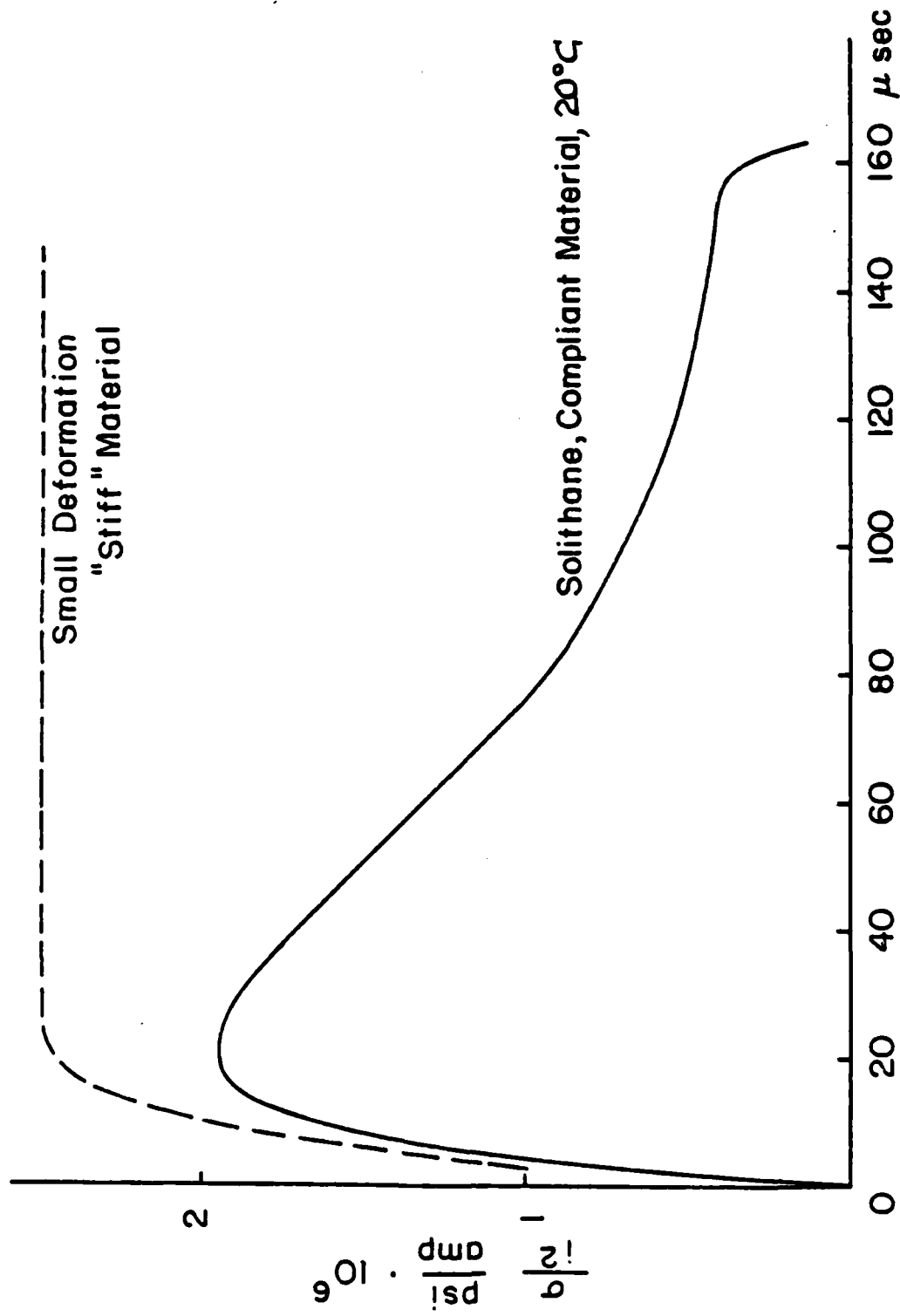
Figure 7. Pressure loss attributed to specimen compliance.
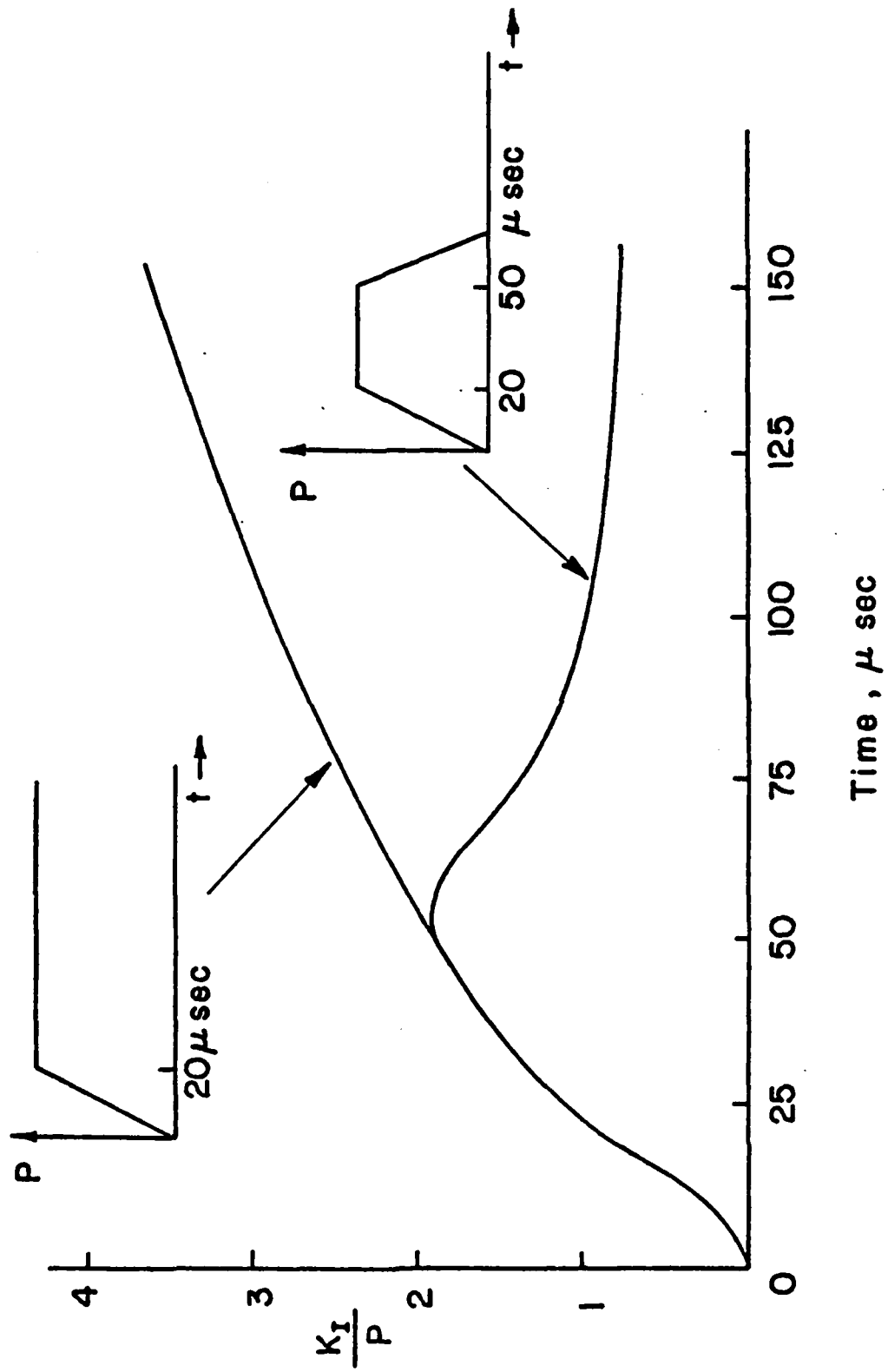
Figure 8.   Estimated stress intensity factor resulting from pulse of finite duration.
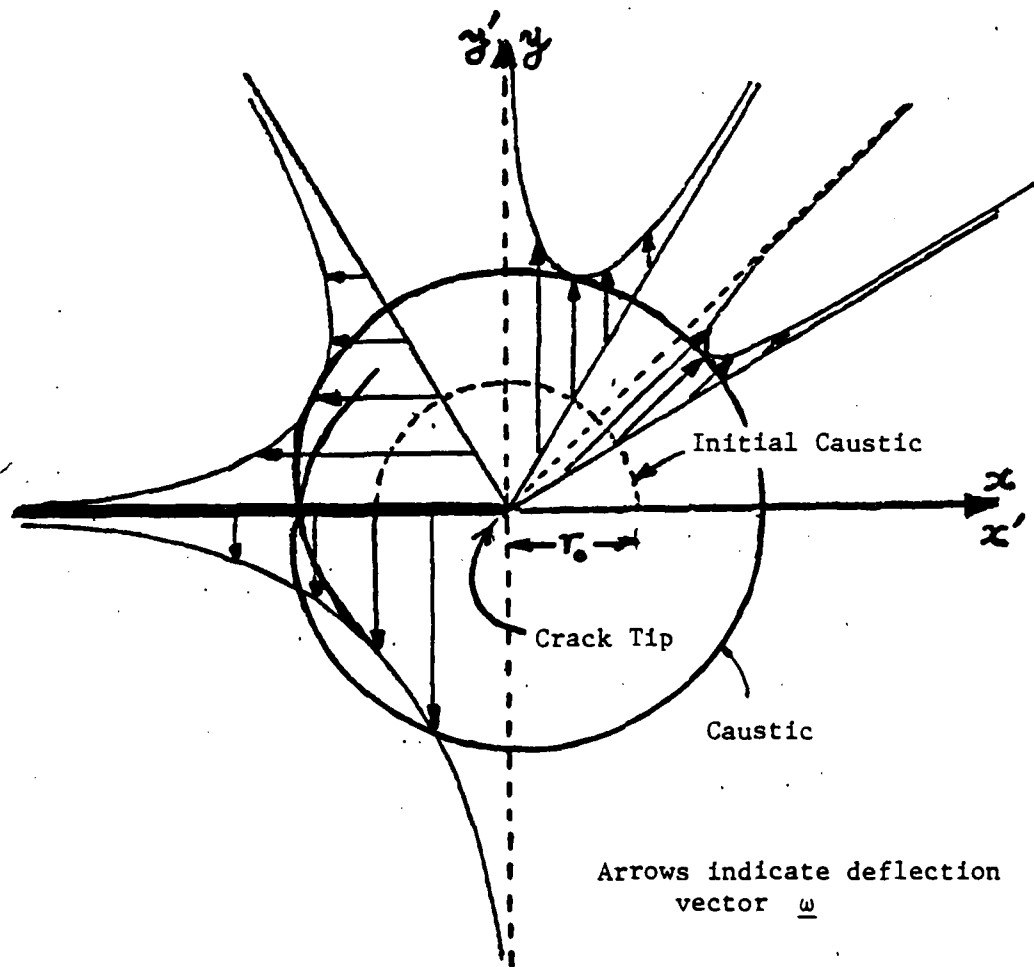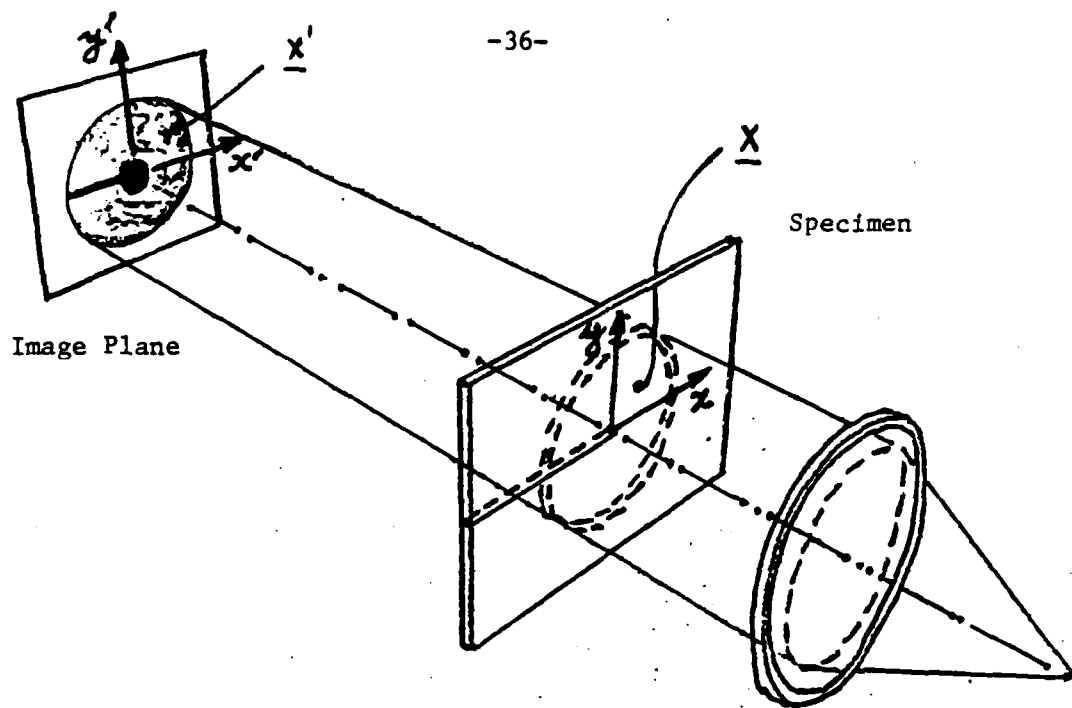
Figure 9.   Optical method of caustics.

-10°C

before
loading

6 sec

12 sec

24 sec

1 min

1.5 min

2 min

3 min

5 min

7.5 min

10 min

15 min

20 min

27 min
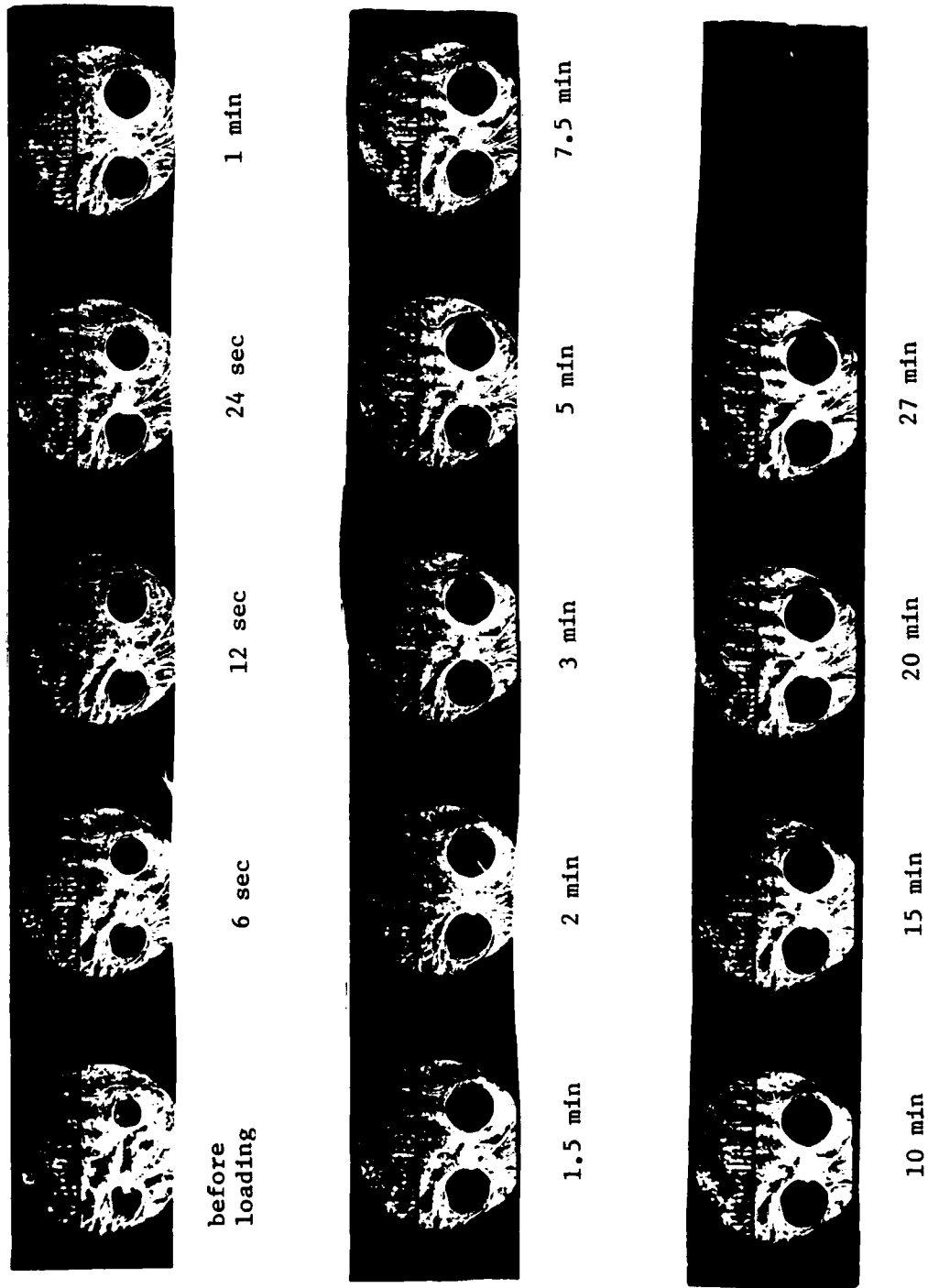
Figure 10. (a) Caustic growth in Solithane 113 at -10°C (stationary crack).
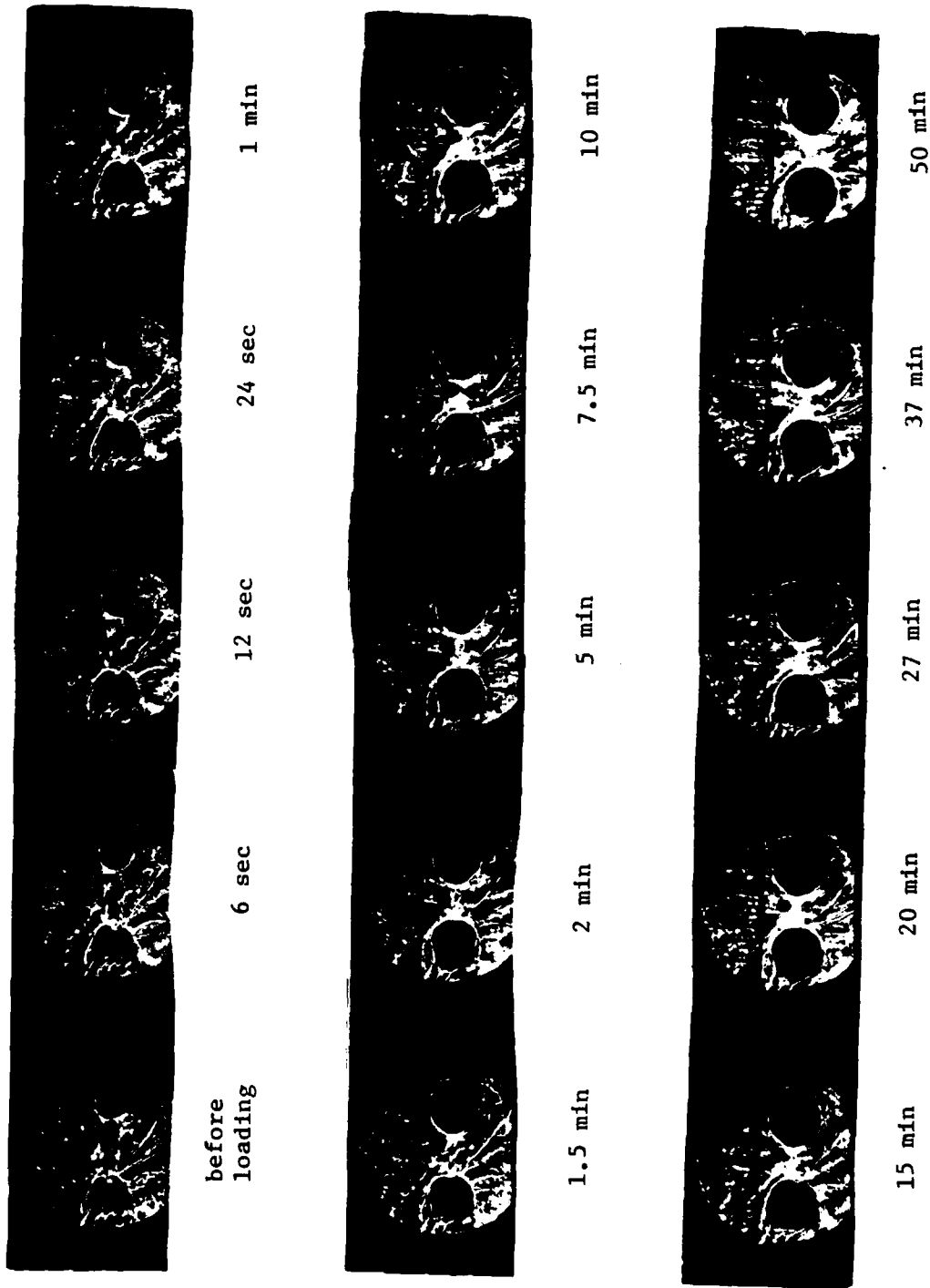
Figure 10. (b) Caustic growth in Solithane 113 at −15°C.
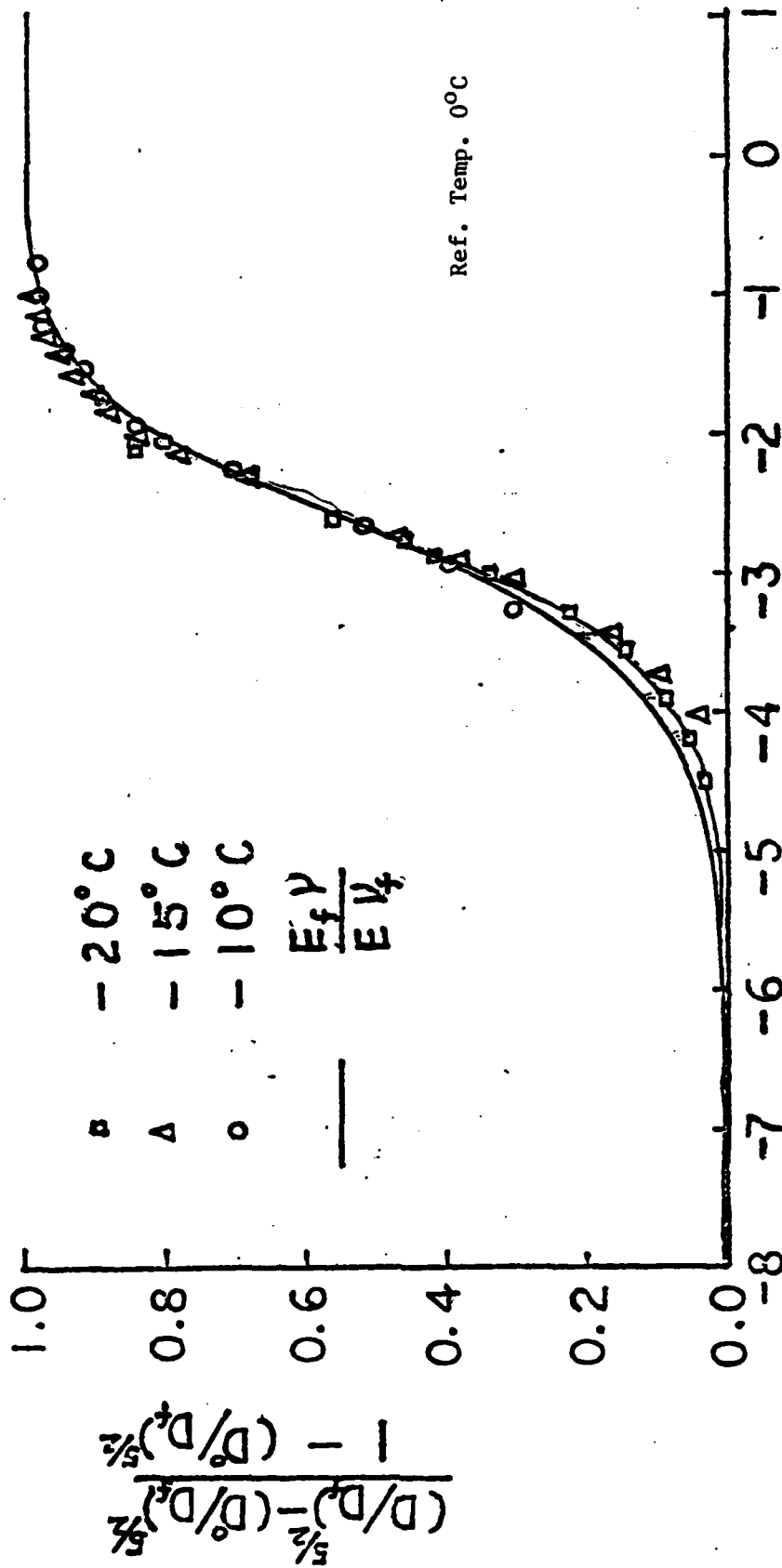
Figure 11. Caustic growth curve for Solithane 113.
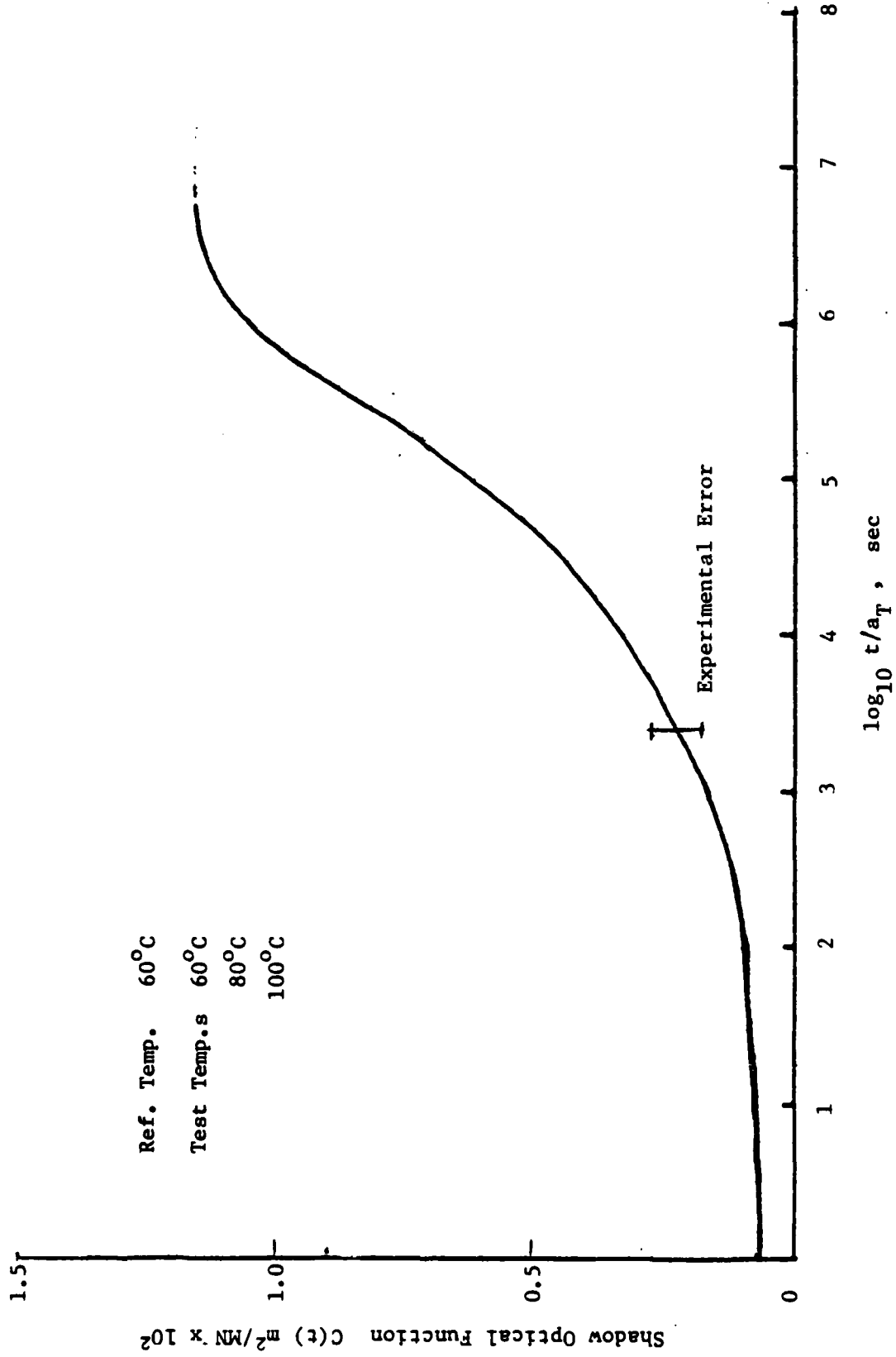
Figure 12. Shadow optical function C(t) for Homalite 100.
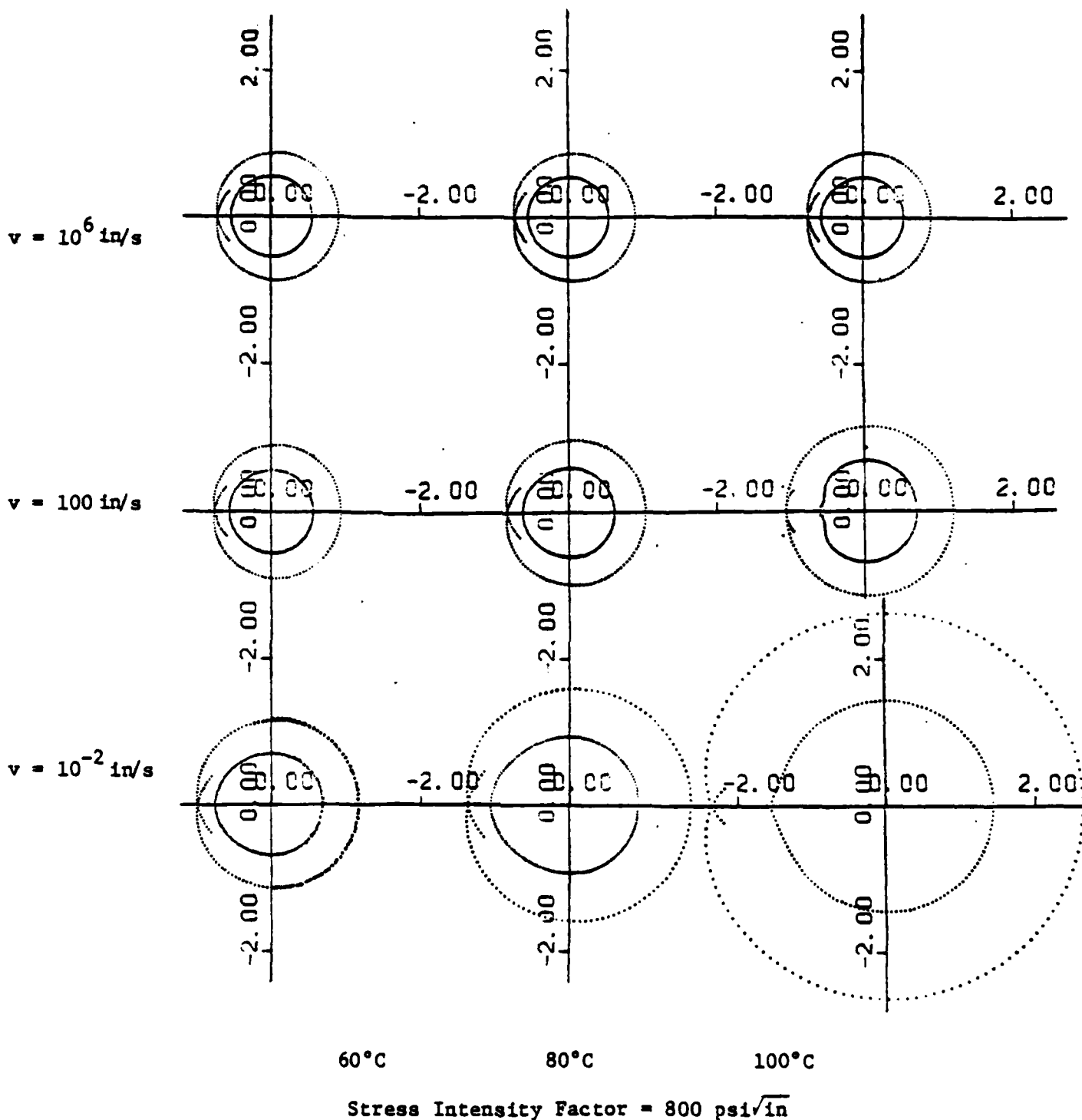
Figure 13. Initial and caustic curve for different speeds and temperatures.
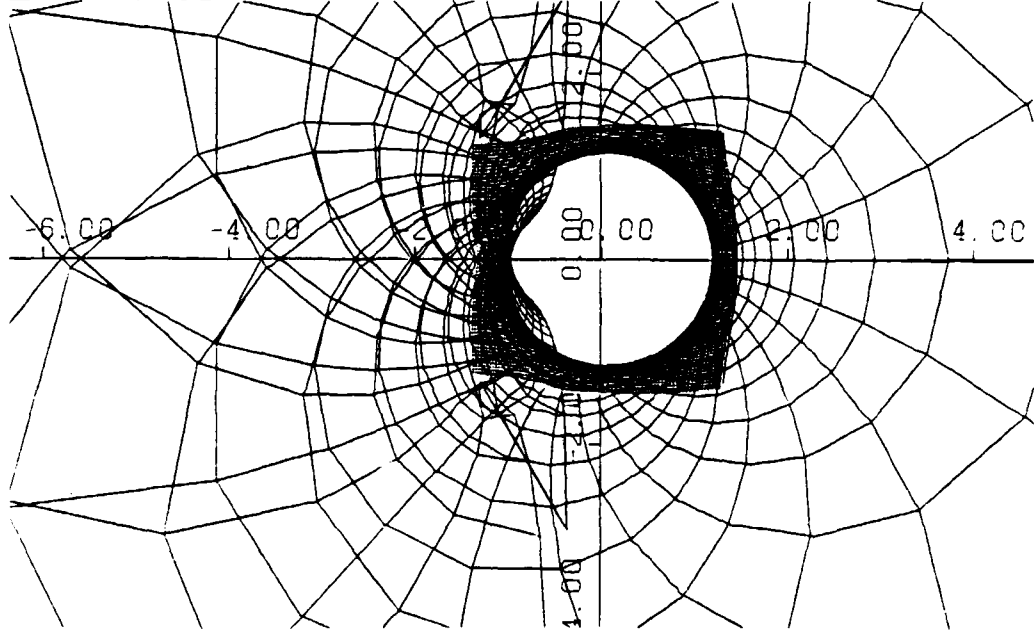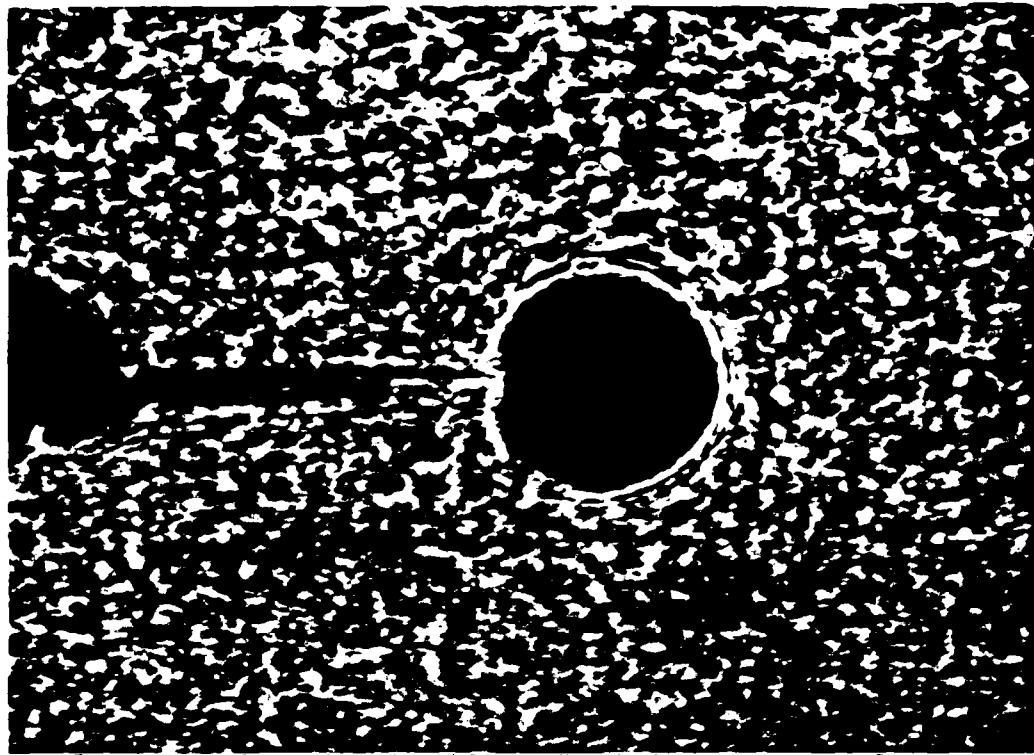
Temp = 100°C, K = 1234 psi(in)$^{\frac{1}{2}}$, v = 9414 in/sec

Figure 14. Comparison of numerical caustics to experimental caustic for a running crack in a Homalite-100.
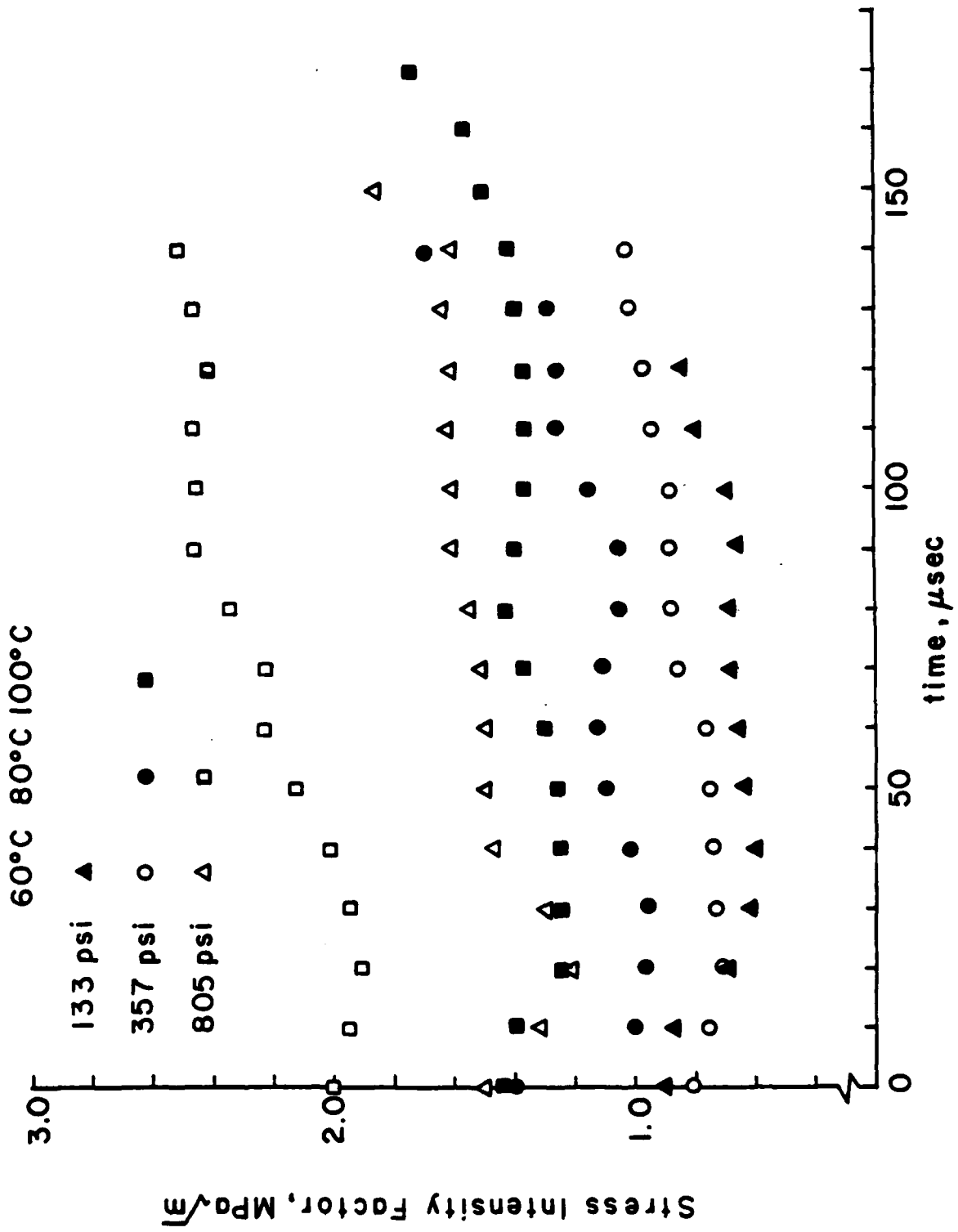
Figure 15a. Stress intensity variation after dynamic crack initiation in Homalite 100.
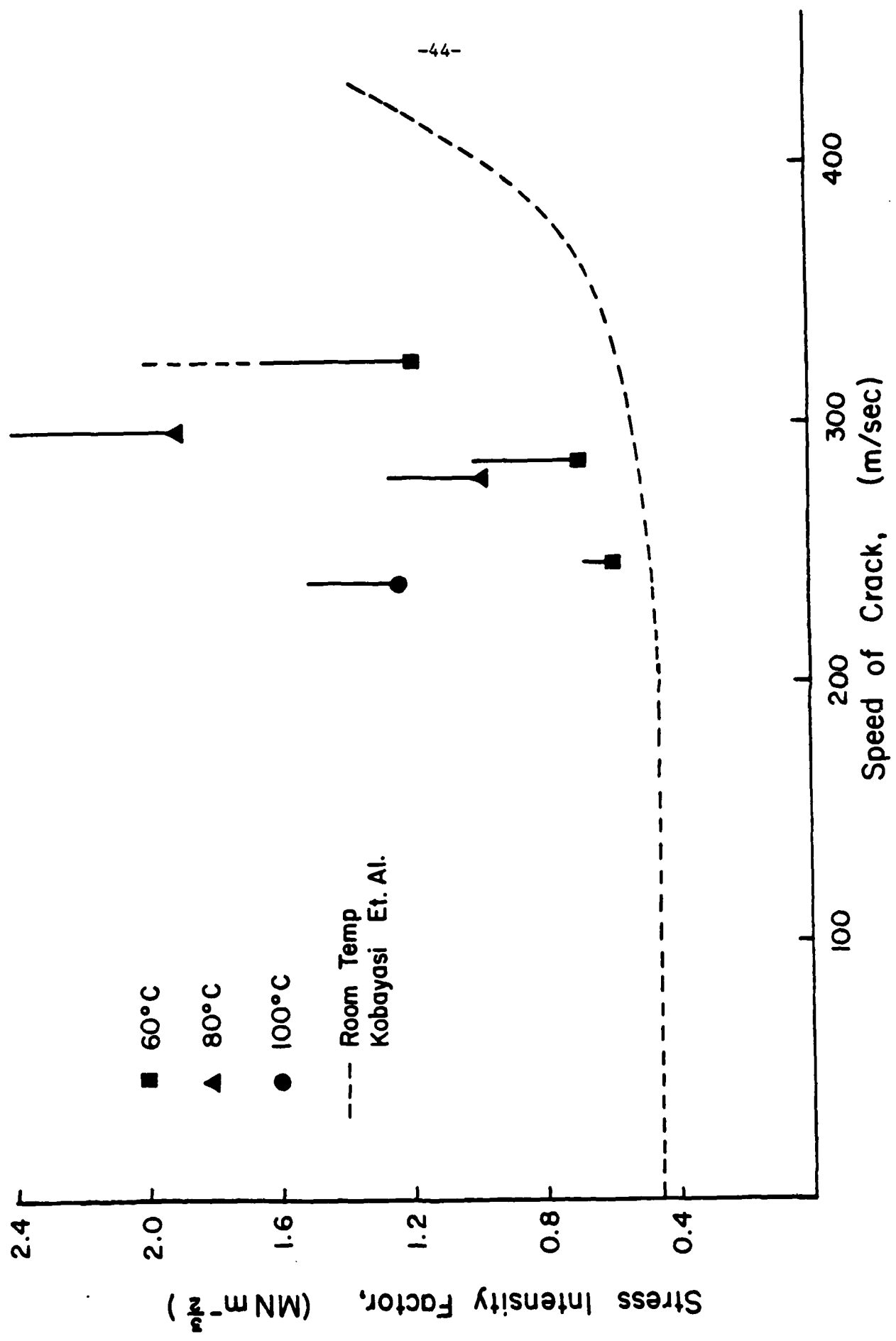
Figure 15b. K-v relation of Homalite 100 at various temperatures.
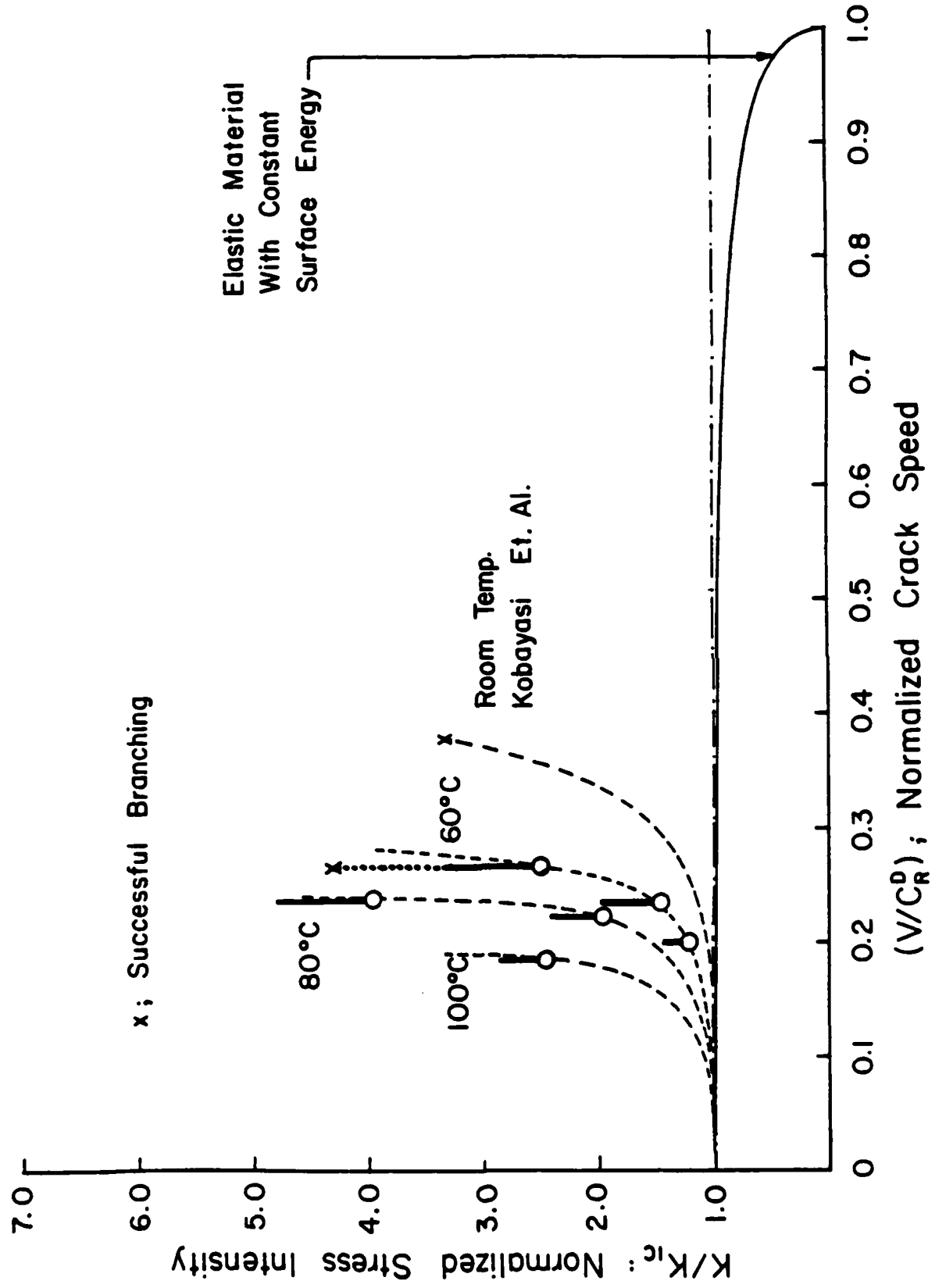
Figure 15c. Normalized K-v relation of Homalite 100 at various temperatures.
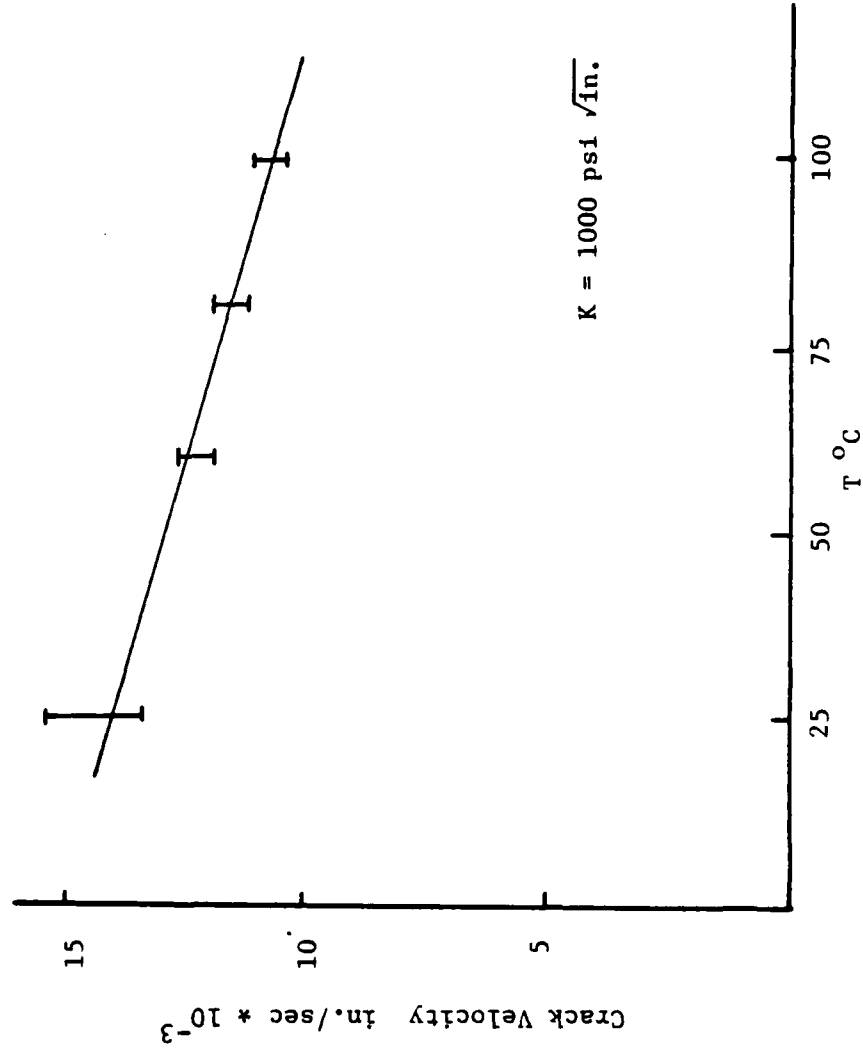
Figure 16. Sensitivity of crack speed in Homalite 100 to temperature.
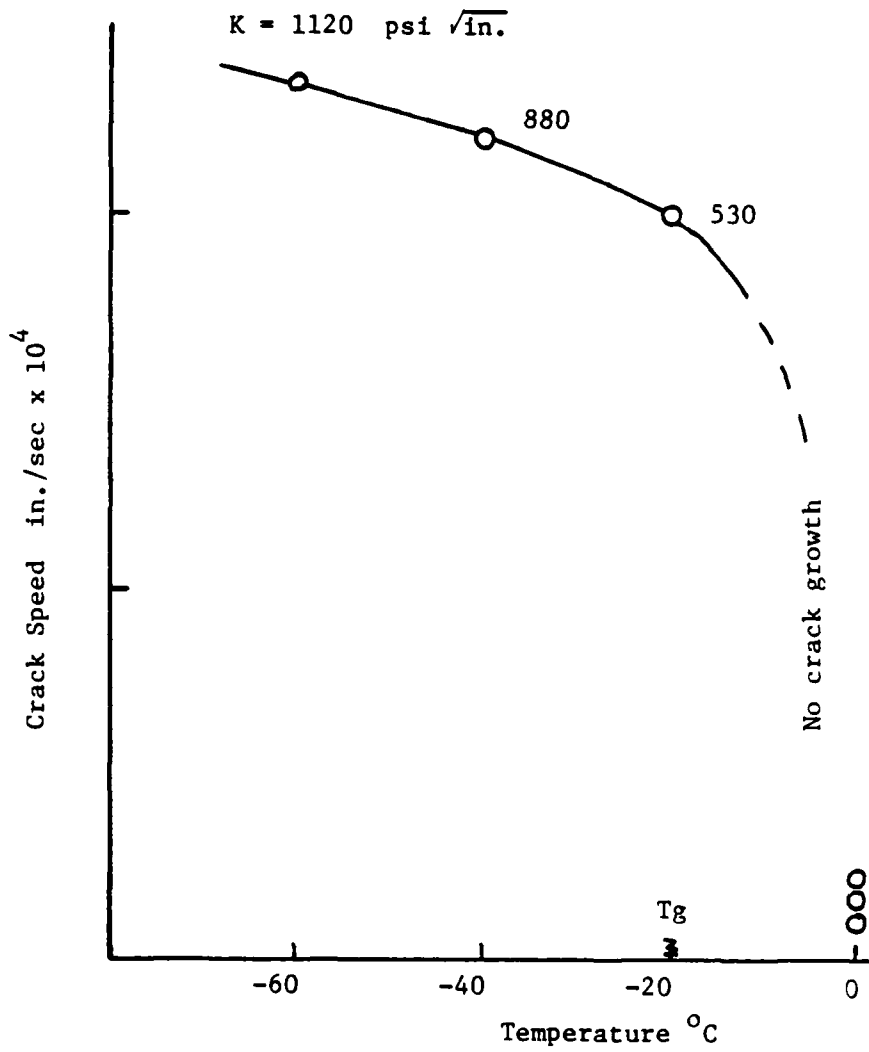
Figure 17. Effect of temperature on crack speeds in Solithane 113.
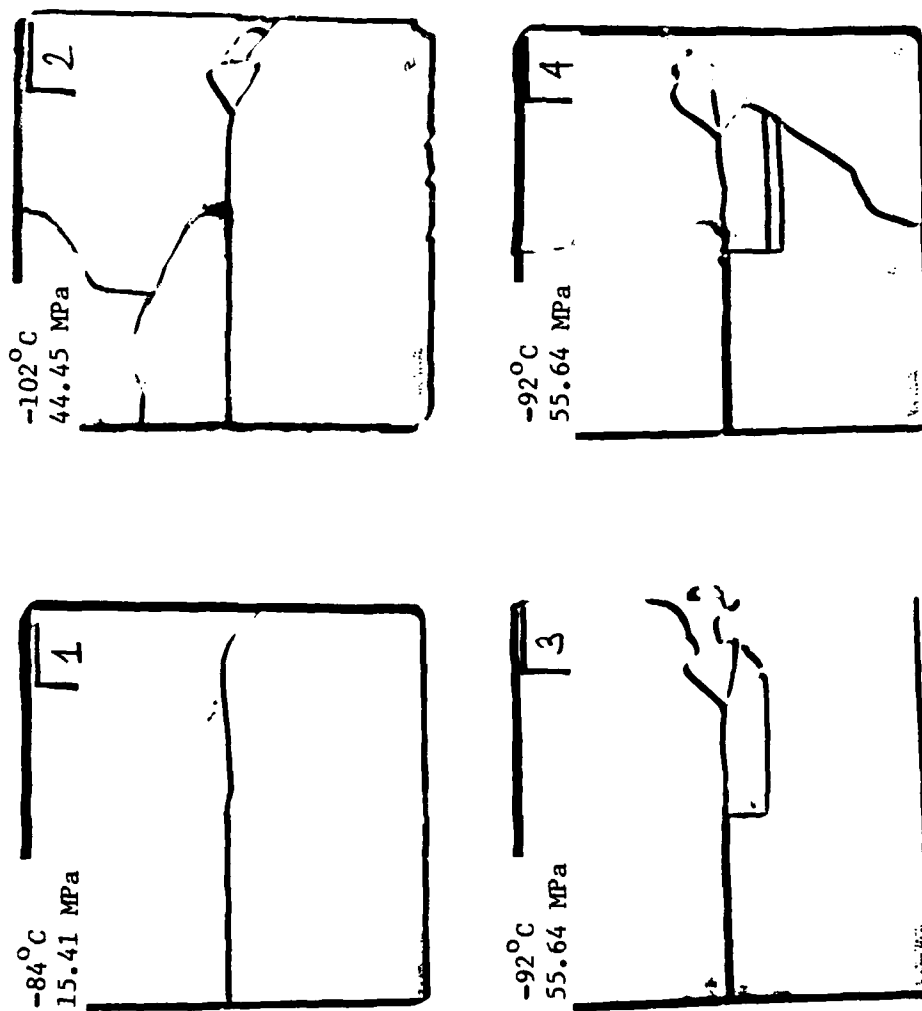
Figure 18. Solithane specimens showing the fracture pattern at various load levels.
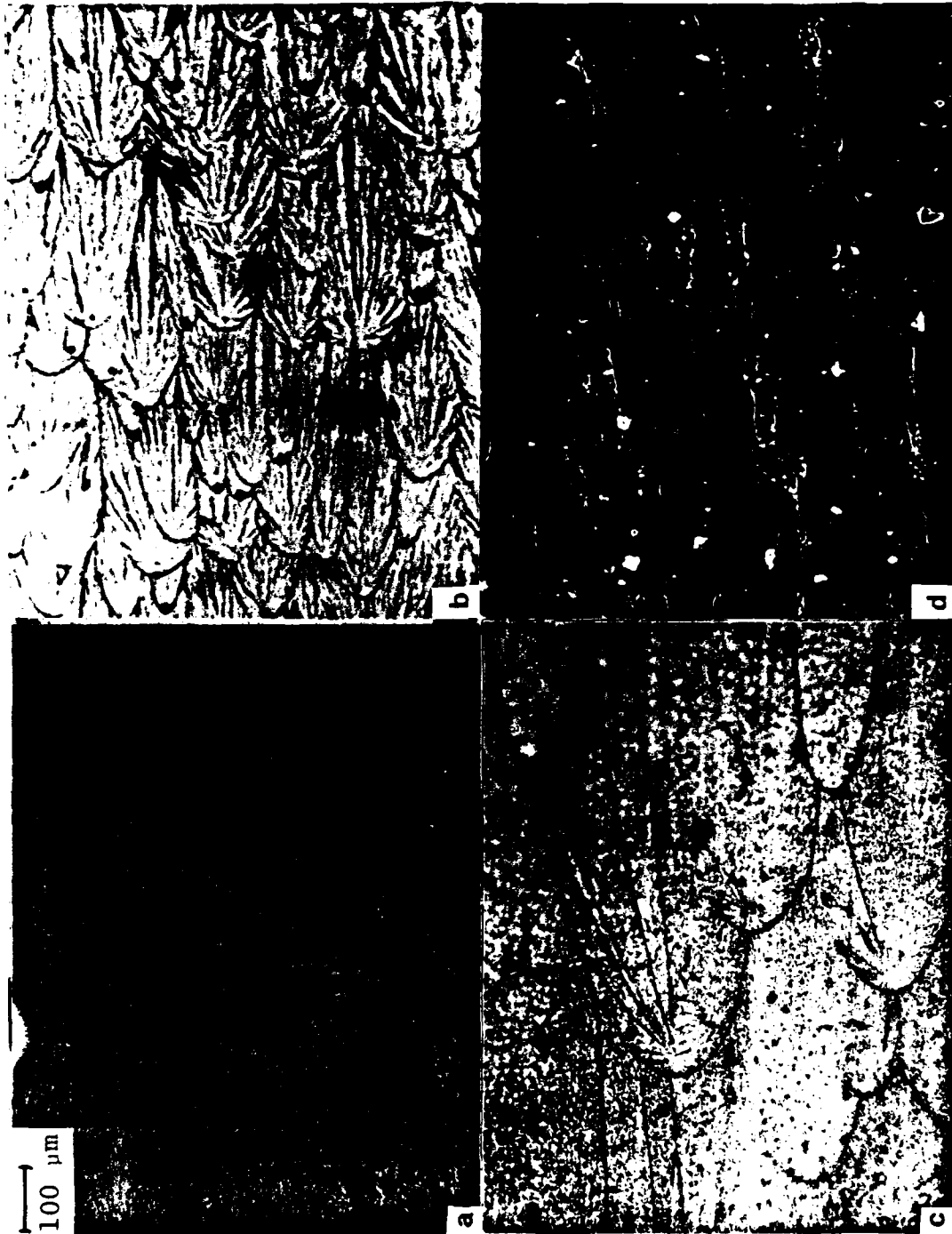
Figure 19. Fracture surface morphology: (a) quasi-statically generated surface in Solithane-113, (b) dynamically generated surface in Solithane -113, (c) dynamic; Plexiglas, (d) dynamic; Homalite 100.
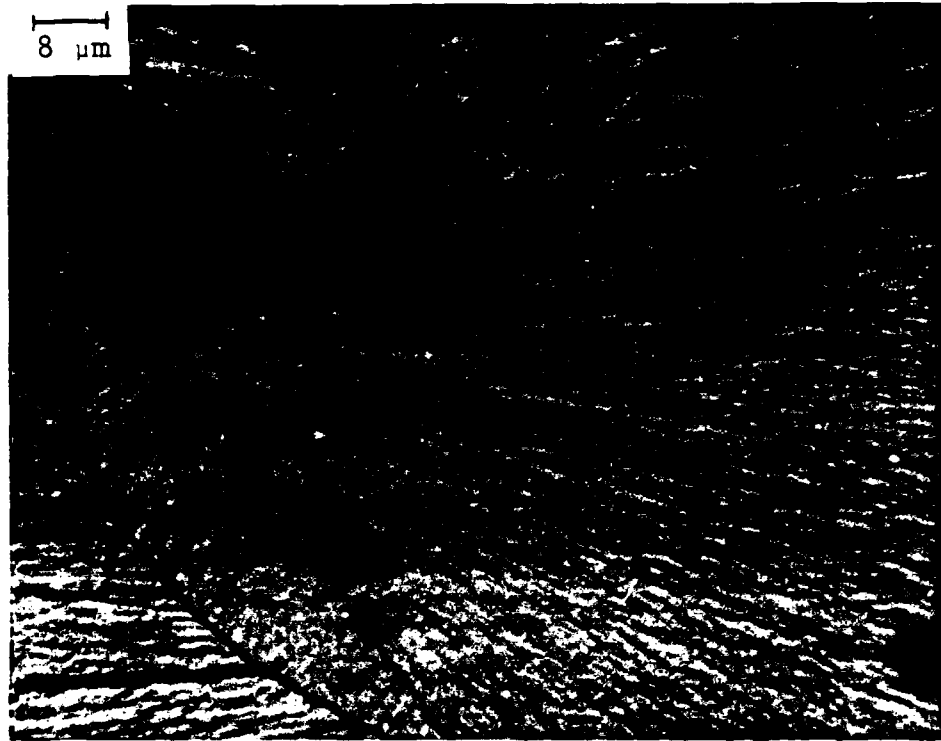
Figure 20. Magnified view of parabolic marking.
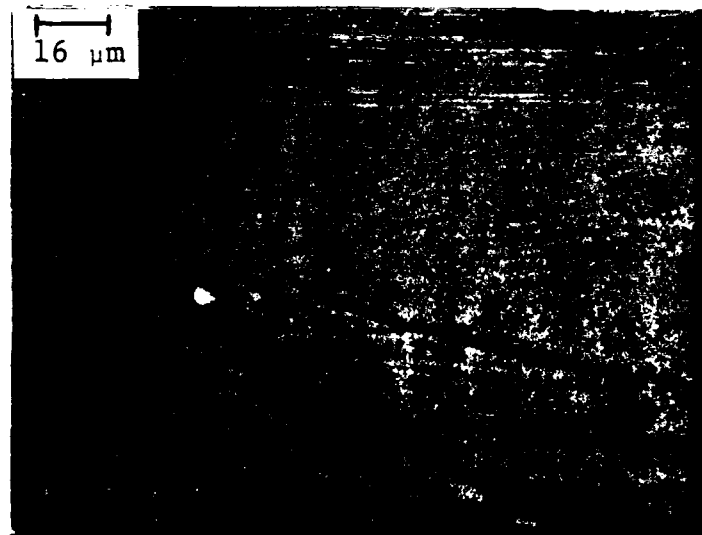
Figure 21. Coalescence of microcracks.
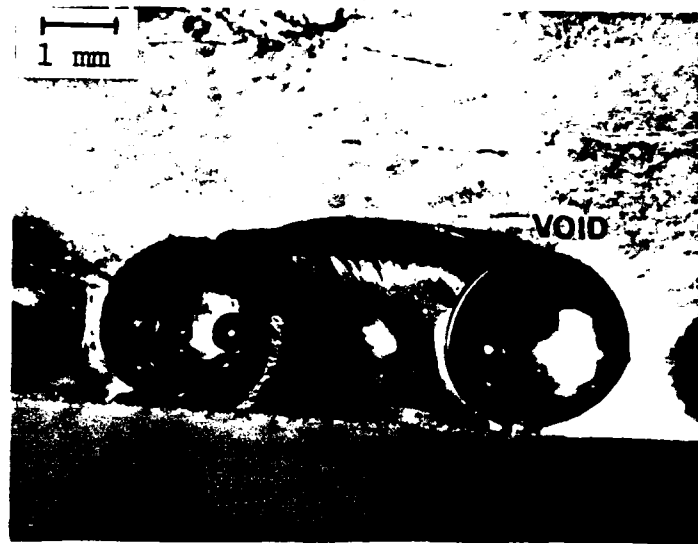
Figure 22. Effect of voids on crack propagation.
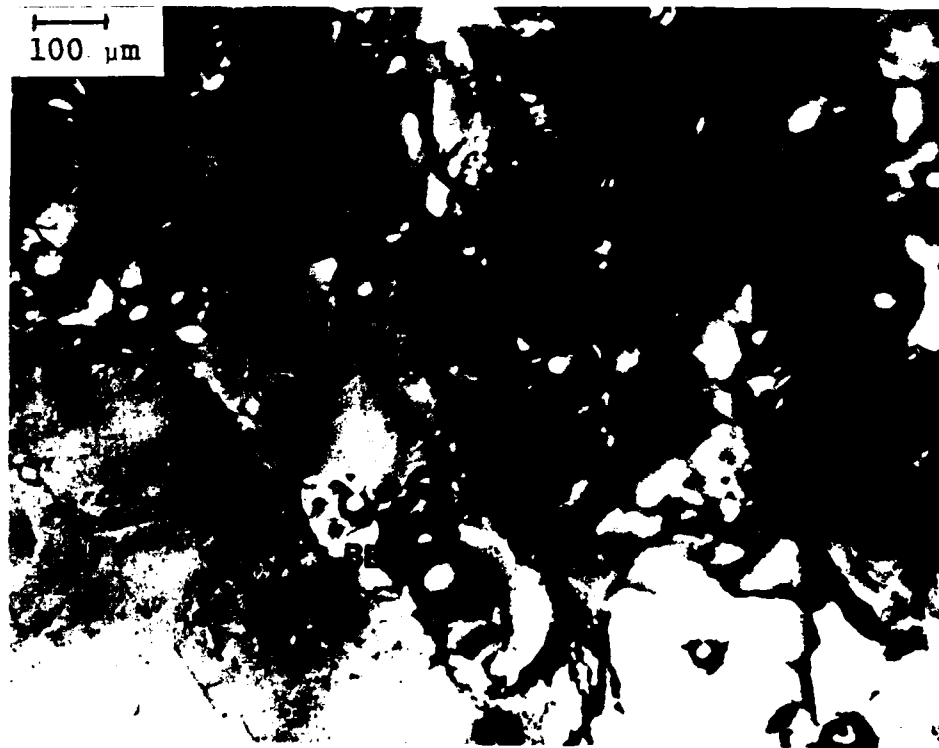
Figure 23. Effect of glass bead filler particles.

APPENDIX: INTRODUCED INHOMOGENEITIES

The micro-mechanics of fracture are greatly influenced by material imperfections, or inhomogeneities. In particular, an understanding of the fracture mechanics of highly filled materials is possible only through an understanding of such micro-mechanical interactions.

Introduction of large numbers of flaws or of a high density of fill material changes the transparency of the test panel so that the method of caustics can no longer be employed. This problem is overcome by having a well defined and localized region of flawed or filled material included in an otherwise pristine panel. In this way caustic data is available just before and just after the crack has passed through the inhomogeneous region. Also, it makes the microscopic comparison of the fracture surfaces in a flawed and in an unflawed region more direct. The behavior in the flawed region is effectively bracketed by the behavior in the pristine material before and after.

Introducing flaws into a test panel after it is cast becomes a rather difficult task except in the case of very large flaws. Introducing small voids into the material, almost inevitably, necessitates that they should be introduced as part of the casting process. Further, any technique developed for including voids can be immediately applied to an inclusion of solid filler particles.

Most polymer substances exhibit a fair amount of cohesion. Even silicone rubbers, which are noted for their lack of adhesion, will bond to previously cured pieces of silicone rubber. This general tendency is useful when casting with polymers. It is not always necessary to cast the entire object at once. The casting can take place in steps as long as scrupulous cleanliness is maintained.

Gravity can cause undesirable setting out in castings of two insoluble substances mixed together. A slow rotation of the mold can alleviate this problem if

the mixture is viscous enough and the cure time is short enough. Such an arrangement is useful when casting inhomogeneities into a test panel. Utilizing this technique as well as the above mentioned technique of casting in parts, it has proved possible to cast a small well defined region of inhomogeneous material into a large otherwise homogeneous panel. A great deal more control over the final product can be exercised using this process. The procedure has been used in Solithane panels with quite reasonable results. Figure A1 is a photograph of a glass and metal mold used to cast the small inhomogeneous region. The casting from this particular mold are 2.5 inch in diameter while the inclusion of inhomogeneous material has generally been limited to a 1 inch diameter zone in the center. The 2.5 inch diameter discs are then cast into full size 12"x12" panels of the same thickness. Any of the dimensions mentioned can be varied with relative ease. Castings have been made with various sizes and densities of air bubbles or glass beads introduced.

A 1.   Mold for casting inserts with voids or filler particles.

END

FILMED

11-85

DTIC